2014

Analysis Of Debris From Implant Prostheses

Mehran Varedi
University of Alabama at Birmingham

ANALYSIS OF DEBRIS FROM IMPLANT PROSTHESES

by

MEHRAN VAREDI

PERNG-RU LIU, COMMITTEE CHAIR
JACK E. LEMONS
DANIEL A. GIVAN
KEITH E. KINDERKNECHT
AMJAD JAVED

A THESIS

Submitted to the graduate faculty of The University of Alabama at Birmingham,
in partial fulfillment of the requirements for the degree of
Master of Science

BIRMINGHAM, ALABAMA

2014

ANALYSIS OF DEBRIS FROM IMPLANT PROSTHESES

Mehran Varedi

Dentistry

ABSTRACT

Objectives: The specific aim of this study was to analyze any entrapped debris in implant abutment screw threads from post processed constructs from dental laboratories. Materials and Methods: Forty implant screws were used to collect debris where screws were removed from the implant prosthesis as received from dental laboratories. In all samples, laboratory procedures including fabrication of the custom abutment, definitive prosthesis and finishing/polishing were completed prior to sampling. Twenty-nine screws were from titanium and eleven screws were from zirconia abutments. Scanning Electron Microscope (SEM) analyses of collected particulate products from abutment screws were done for all specimens. Results: The SEM analysis showed multiple particles with different sizes, shapes and chemistries. Elemental analysis of these particles supported that their origin was from the abutment/prosthesis or transferred from other sources utilized in the dental laboratories during the fabrication processes. Conclusion: Based on the results it was concluded that particles on abutment screw surface were present and their characteristics may affect the abutment implant joint stability and/or may have a biological effect on peri-implant tissue health. Therefore a consistent method of cleaning is needed for abutment screws before clinical use of any screw and prosthesis received after processing by dental laboratories.

Keywords: Implant, Screw, Abutment, Contamination, Debris

TABLE OF CONTENTS

Page

LIST OF TABLES

Table Page

LIST OF FIGURES

Figure Page

Figure Page

Figure Page

Figure Page

Figure Page

INTRODUCTION

Implant screw contamination with debris may happen during laboratory procedures and clinicians may receive implant prosthesis with debris on the surface. This debris may have a negative mechanical and chemical impact on implant joint stability. These particles may also cause a negative tissue reaction, if transferred into the region.

One of the most critical factors on implant joint stability previously studied[8] is preload. When tightening torque is applied to an abutment screw, the component parts are compressed together and the screw elongation results in tension. The stretched screw, when deformed elastically, pulls the segments together creating a compressive clamping force. These forces are designated as the "preload". The preload in the screw, from elongation and elastic recovery, is the result of the combined clamping force[1,3,4]. Screw joint stability is achieved when the clamping force exerted by the screw exceeds the joint separating forces acting on the assembly[8].

The actual preload achieved in the components is dependent on the torque applied plus the finish of the interfaces, friction between components, geometries, and various material properties. Even within the same lot of prosthetic components, there may be significant differences in the preload achieved because of the factors listed above[2]. Also several factors may affect maintaining preload after loading the implant prosthesis. These factors as listed includes applied torque plus direction of force, connection type and design, component material surface topography, fit, and time dependent effects between contact surfaces such as creep[5,6,7]. Since the quality of mating surfaces in screw joint will

influence the preload, any kind of debris at the mating surfaces of the joint may cause an imprecise fit and may reduce the magnitude of the preload.[1]

Some previous studies have been provided on the effect of particles resulting from corrosion or prosthetic wear on peri-implant tissue response. Galvanic corrosion between different metallic particles and titanium and consequent release of metallic ions has been shown to have cytotoxic potency and possibly cause immune reactions[15]. Also, the soft tissue stability around implant abutment interface affect marginal bone as well. Literature shows interactions between cellular components and implant abutment materials that influences the stages of the healing around implants[9 10]. For example, micrometer sized titanium particles have been shown to influence the inflammatory process[11].

Cleaning procedures of implant abutments using ultrasonic and plasma devices have been suggested [9 11]. In a study by Canullo et al. customized titanium abutments were studied after different cleaning procedures using plasma and ultrasonic treatments and results showed beneficial cleaning after laboratory technical stages completed on abutments. Their study showed that cleaning with steam did not clean the contamination as effectively as ultrasonic or plasma methods[9].

In the current study, analysis of entrapped debris along implant screw threads and connections was investigated. These debris were collected from implant screws returned from dental laboratories and analyses include debris size, shape and chemistry. It was hypothesized that SEM analysis of entrapped debris along implant screw threads and connections will show different particle shapes, sizes and elemental chemistries.

MATERIALS AND METHODS

Implant Abutment Screw

This in vitro study included forty screws to collect debris. All of screws were removed from the implant prostheses, as received from the dental laboratories. In all samples, laboratory procedures including fabrication of the custom abutment and definitive prosthesis were completed and definitive prosthesis was intended for clinical placement. Two groups of screws were evaluated in this study.

Group A screws were collected from ZrO2 abutments with a titanium base. In this group all definitive restorations were all ceramic restorations (Table 1).

Group B screws were collected from titanium abutments with definitive PFM restoration (Table 2). From the forty screws, twenty-nine screws were from titanium custom abutments and PFM restorations and eleven screws were from ZrO2 custom abutments with full ceramic restorations.

In the ZrO2 group the definitive prosthesis included eight IPS Emax crowns, one porcelain fused to zirconia, one Yttrium Stabilized Zirconia YZr and one BruxZir (full Zirconia crown). Implant systems were from different manufacturer (Tables one and two).

Table 1. Group A Screw Samples Collected from ZrO2 Abutments; Implant System and Restoration Type

SAMPLE	IMPLANT SYSTEM	RESTORATION TYPE
1	STRAUMANN BONE LEVEL	EMAX
2	STRAUMANN BONE LEVEL	EMAX
3	STRAUMANN BONE LEVEL	EMAX
4	STRAUMANN BONE LEVEL	EMAX
5	STRAUMANN BONE LEVEL	EMAX
6	NOBEL ACTIVE	EMAX
7	NOBEL ACTIVE	BRUXZIR
8	NOBEL REPLACE	EMAX
9	ZIMMER	LAVA (PFZ)
10	3I	EMAX
11	BIOHORIZONS	FORTE YZR ZIRCONIA

Table 2. Group B Screws Collected from Titanium Abutments with PFM Restorations; Implant System and Number of Screws

IMPLANT SYSTEM	NUMBER OF SCREWS
STARUMANN BONE LEVEL	18
STRAUMANN TISSUE LEVEL	2
NOBEL REPLACE	3
NOBEL ACTIVE	2
ZIMMER	2
3I	2

Debris Collection and Weight

In the present study, the method used to collect debris from samples was placement of screws inside a glass tube containing ethyl alcohol followed by placing glass tube inside an ultrasonic cleaner for ten minutes. To evaluate the efficacy of this method a sample screw was evaluated by SEM before and after cleaning (Fig 1)

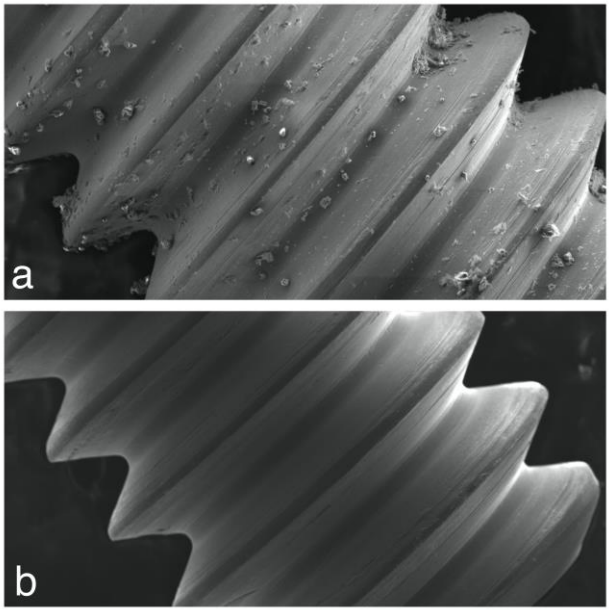

Figure 1. SEM micrograph showing implant abutment screw surface before cleaning (a) and after cleaning (b)

The removed screws were placed inside a glass tube containing ethyl alcohol. Separate glass tubes were used to collect debris from samples with titanium and zirconia custom abutments (Fig 2a). The glass tube was placed inside an ultrasonic cleaner device and after running the ultrasonic device for ten minutes, the screw was removed and washed using ethyl alcohol with a syringe to ensure maximum removal from the screw surface. The glass tubes containing debris collected from twenty-nine screws from the titanium abutment group and eleven screws from the zirconia custom abutments were centrifuged at 3000 RPM for 5 minutes. The glass tube caps were then removed allowing the alcohol

to evaporate at room temperature (Fig 2b). A weight scale unit with 1/10000-gram resolution was used to measure debris weight from each sample group. Deducting the weight of the empty glass tube from the glass tube containing debris was done in order to measure the weight of each sample.

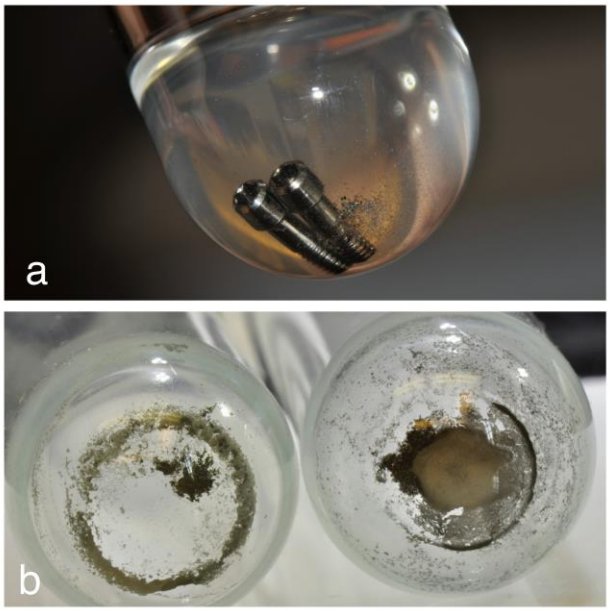

Figure 2. Photographs showing (a) abutment screws inside glass tube containing ethyl alcohol and (b) collected debris from group A screws (left) and group B screws (right)

To prepare the samples for evaluation by SEM, ethyl alcohol was added inside the glass tubes containing debris and the tubes were placed in ultrasonic device running for 10 minutes to re-suspend the debris within the alcohol.

SEM Procedure and Qualitative Measurement of Debris Shape, Size and Elemental Chemistry

The debris from each group was evaluated using SEM for analysis of collected particles. Standard aluminum SEM specimen mounting stubs were used to hold the samples. After adding alcohol to the glass tubes and ultrasonic processing, the suspension of particles was transferred by pipet to the SEM mounting stubs. The particle suspensions were

placed on the stub and the solvent was allowed to evaporate, depositing the particles on the surface. A flow of warm air over the surface, during the solvent evaporation also helped provide a dispersal of the particles. After evaporation of alcohol no coating was applied on the surface of the samples.

In the present study, a QUADRO FEG 650 SEM unit was used with settings of 30kv accelerating voltage and the magnification was varied from 200X to 8000X for studies. A total of 14 fields of view micrographs were saved in TIF format. In each field of view, several spots were selected to analyze the elemental chemistry of particles selected by color and geometry. The samples were evaluated to identify areas with different particle sizes, shapes and colors. Also each sample was evaluated at lower magnification to identify the largest particles.

RESULTS

Two specimens from debris collected in tubes A and B were prepared for evaluation by Scanning Electron Microscope (SEM) energy dispersive x-ray (EDX) analysis. A total of 14 scanning electron micrographs were taken from samples which include 7 micrographs from group A (Figures 3a to 9a) and 7 micrographs from group B (Figures 10a to 16a). The SEM analysis showed contaminant particles with different size, shape and chemistry. The weights of particles measurements did not show a difference in the weight of glass tubes with and without debris.

Debris Morphology Observations

Samples were evaluated using magnifications from 200X to 8000X to identify the debris morphology (size, shape and color). The particles were found to be non-uniform in size and shape and color

Group A Debris Morphology

The SEM analysis of the group A sample demonstrated the presence of a variety of particles with different morphological characteristics (Figures 3a to 9e). After evaluation of the sample the largest particles were found to be in the range of 200-300 micrometers (Fig 8a). The number of these large particles in the whole sample was limited (less than 5).

The smallest particles were less than one micrometer (Figures 4a, 7a and 9a). After evaluation of the test samples, most particles were less than 50 microns in size. The shape of particles was also found to be very different. They were spherical, rounded or angular, twig, fibrous, flake or cylindrical (Figures 3a to 9a).

Group B Debris Morphology

The SEM analysis of group B sample demonstrated the presence of a variety of particles with different sizes and shapes (Figures 10a to 16a). After evaluation of this sample, the largest particle was found to be approximately 50X600 micrometers (Figure 15a).

The sizes of most particles were found to be less than 50 micrometers and the smallest particles identified to be less than one micrometer (Figures 10a to 16a).

The shape of particles was also found to be very different. Like the previous group, a variety of irregular shapes were found (Figures 10a to 16a). The smaller sized particles were relatively round and spherical compared with the larger particles, which were blocky, fibril and elongated.

SEM-EDX Elemental Analysis

Group A SEM Chemical Analysis

The chemistries of particles were evaluated using different spots in each overall area (Figures 3a to 9e).

The SEM-EDX microanalysis of largest particles in test sample from group A showed that these particles consist mostly silicon, oxygen and carbon (Figure 8b). Also relatively large particles with different chemistry were found (Figures 3a and 3b). The SEM-EDX microanalysis of area 1 spot 1 showed one particle, with a size of 15 by 60 micrometers, which was mainly Ti (titanium).

Major parts of particles were found to have elements such as titanium and aluminum (area 1 spot 1, area 2 spot 1 and 3, area 3 spot 1, area 4 spot 4 and area 7 spot 4), silicon (area 2 spot 2, area 4 spot 2, area 6 spot 1, 2 and 3, area 7 spot 2), carbon (area 3 spot 2, area 4 spot 1 and area 7 spot 1) and zirconia (area 5 spot 1 and 3). Other elements from group A included oxygen, calcium, vanadium, potassium, sulfur, copper and yttrium.

Some elemental traces of iron (Fe), sodium (Na), palladium (Pd), silver (Ag), chromium (Cr), ytterbium (Yb), molybdenum (Mo), nickel (Ni), platinum (Pt), chlorine (Cl), magnesium (Mg), niobium (Nb) and lanthanum (La) were also detected in the debris particulates (Figures 3a to 9e).

Group B SEM Chemical Analysis

The chemistries of particles were also evaluated in different spots in each area for group B (Figures 10a to 16e). The SEM-EDX elemental analysis of the largest particle in test sample from group B showed that the main element was titanium (Figure 15b).

The particles in different fields of view were found to have different chemistries. Major elements that were identified were titanium (area 8 spot 9 and 10, area 9 spot 3, area 10 spot 1,2 and 3, area 11 spot 3, area 12 spot 1 and 2, area 13 spot 1 and 3 and area 14 spot 2 and 5), silicon (area 8 spot 11,12 and 14, area 9 spot 1 and 4, area 10 spot 4, 5 and 6, area 11 spot 1 and 4, area 12 spot 3 and 4, area 13 spot 4,5 and 6, area 14 spot 3 and 4), palladium and silver (area 8 spot 13, area 9 spot 2, area 11 spot 2, area 13 spot 2 and area 14 spot 1). Other elements that were frequently identified in analysis of particles in test sample from group B included aluminum, oxygen, potassium, carbon, magnesium, calcium, sodium, copper, zinc and tin. Some elemental traces of iron (Fe), chromium (Cr), molybdenum (Mo), chlorine (Cl) were also detected in the debris (Figures 10a to 16e).

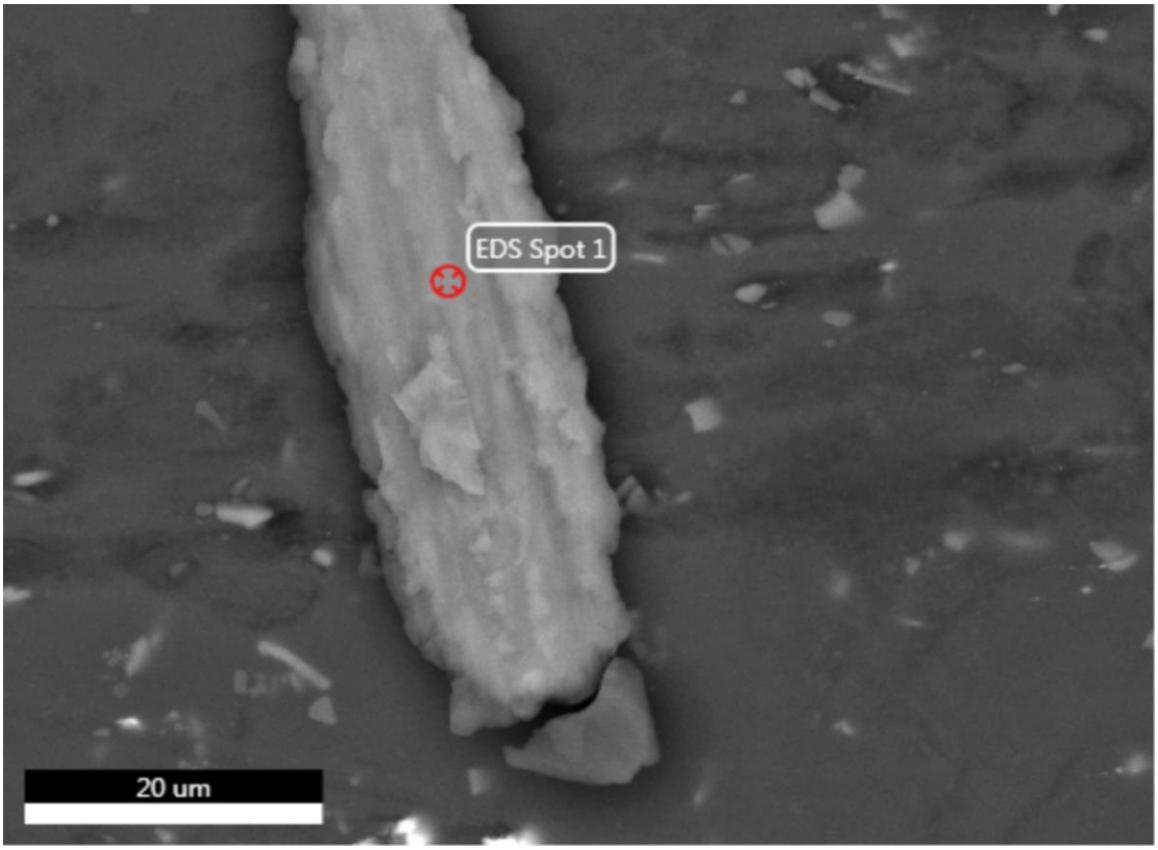

Figure 3a: Micrograph of area 1 showing areas for analysis from group A specimen

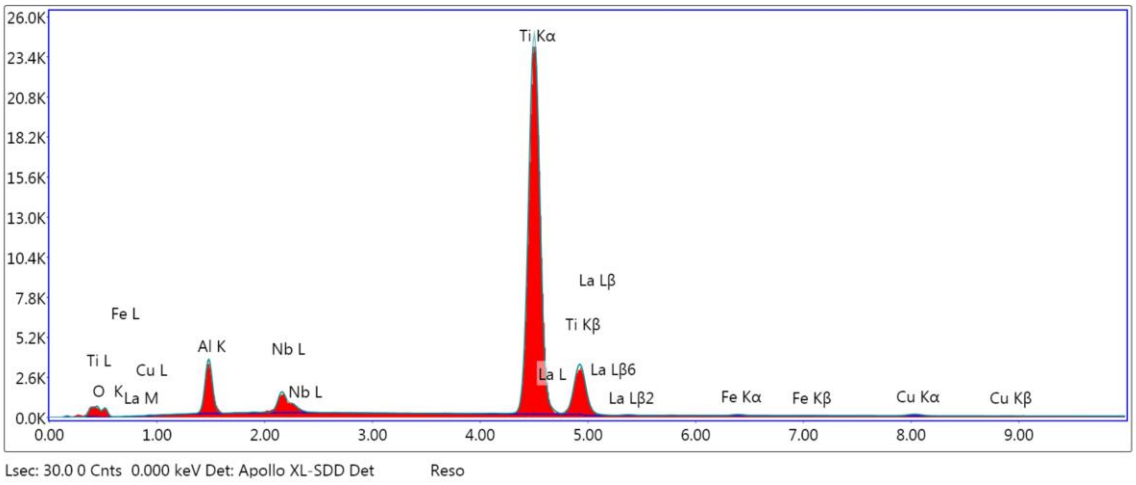

Element	Weight %	Atomic %	Net Int.	Error %
O K	16.05	35.58	121.3	11.79
AlK	9.72	12.78	903.46	8.13
NbL	4.78	1.83	393.25	5.62
TiK	65.37	48.41	10080.26	1.3
LaL	2.99	0.76	154.35	11.44
FeK	0.32	0.2	27.47	23.45
CuK	0.78	0.44	53.37	15.52

Figure 3b: Area 1 Spot 1 element distribution image and quantification from group A specimen

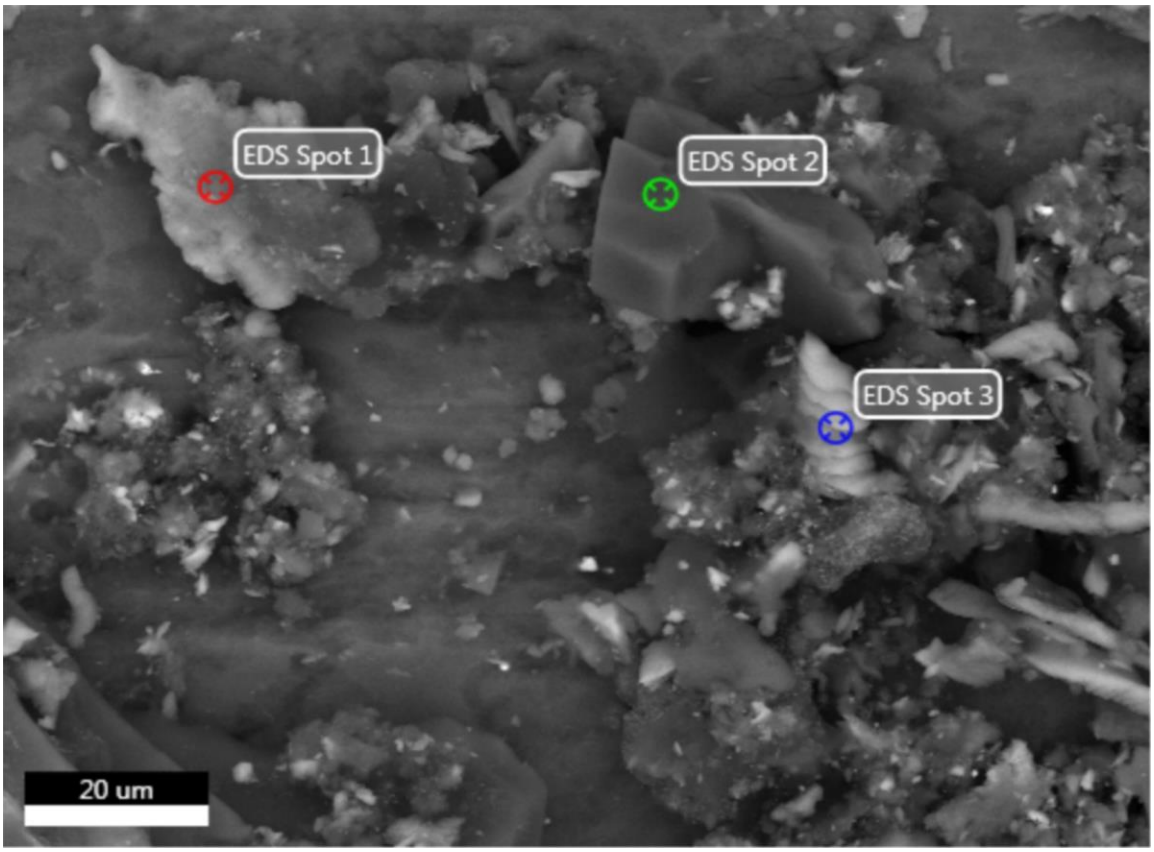

Figure 4a: Micrograph of area 2 showing areas for analysis from group A specimen

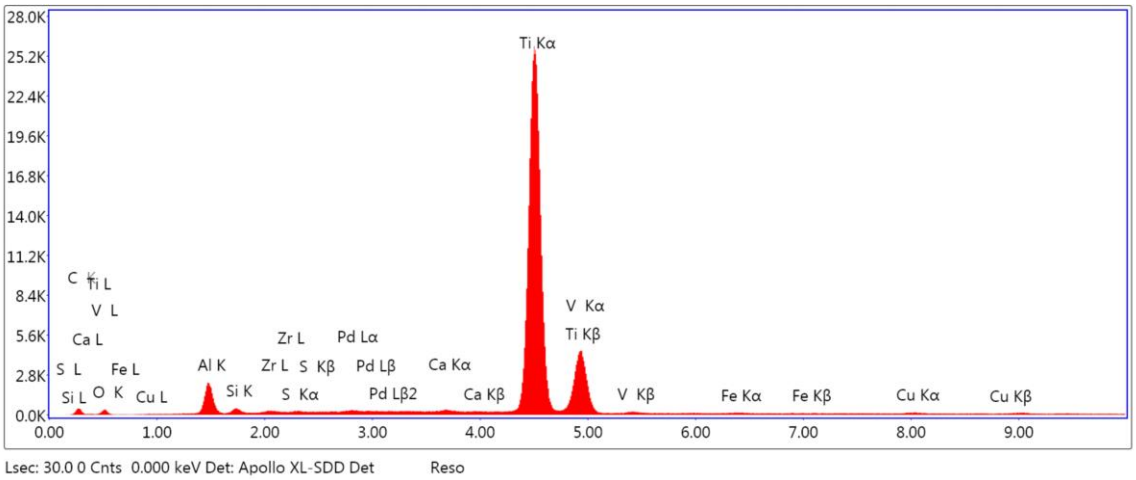

Element	Weight %	Atomic %	Net Int.	Error %
C K	7.5	20	84.24	9.91
O K	11.56	23.13	77.87	12.22
AlK	5.69	6.75	539.37	8.53
SiK	0.28	0.32	35.31	26
ZrL	0.02	0.01	1.24	59.72
S K	0	0	0.68	66.21
PdL	0.15	0.05	19.31	37.14
CaK	0.3	0.24	65.57	13.42
TiK	69.39	46.38	10988.82	0.92
V K	4.12	2.59	544.25	3.02
FeK	0.35	0.2	30.33	27.13
CuK	0.62	0.31	42.24	18.72

Figure 4b: Area 2 Spot 1 element distribution image and quantification from group A specimen

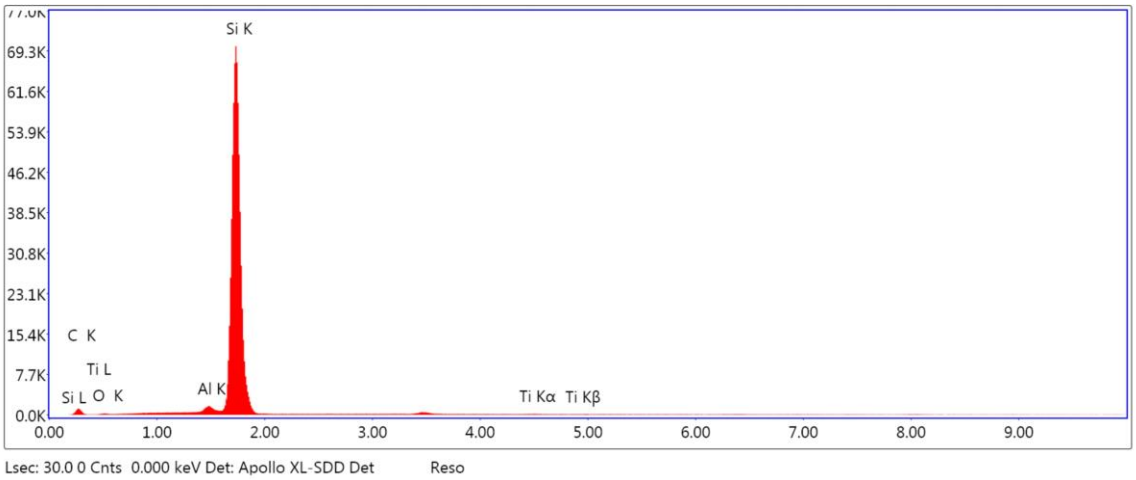

Element	Weight %	Atomic %	Net Int.	Error %
C K	40.72	60.65	249.43	10.71
O K	3.27	3.66	60.44	13.61
AlK	1.36	0.9	476.85	4
SiK	54.55	34.75	20856.74	1.82
TiK	0.1	0.04	22.07	22.62

Figure 4c: Area 2 Spot 2 element distribution image and quantification from group A specimen

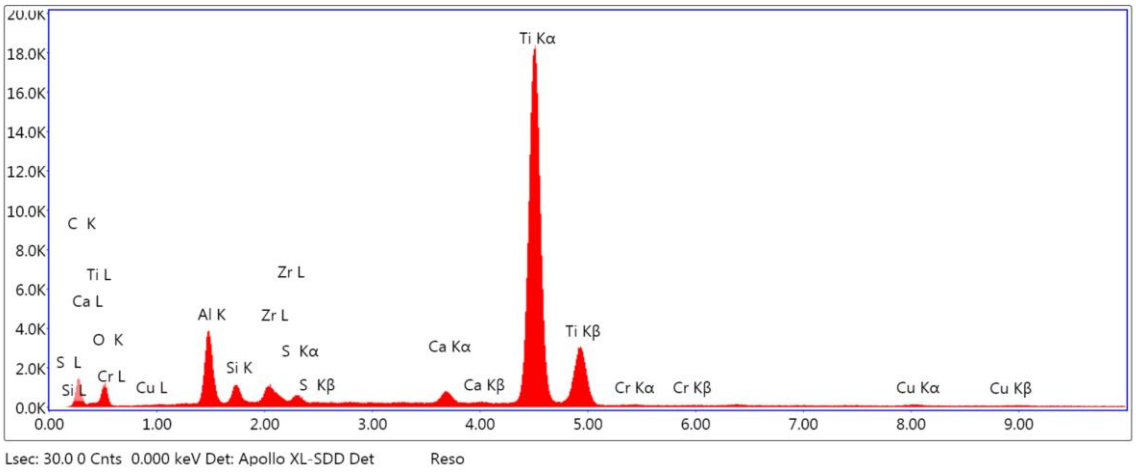

Element	Weight %	Atomic %	Net Int.	Error %
C K	23.01	41.36	293.07	8.86
O K	23.7	31.97	259.18	10.96
AlK	7.3	5.84	1033.48	7.18
SiK	1.45	1.11	249.7	8.09
ZrL	2.39	0.57	248.71	5.6
S K	0.53	0.36	114.73	11
CaK	1.13	0.61	271.83	4.17
TiK	39.94	18	7750.51	1
CrK	0.11	0.04	13.8	30.16
CuK	0.45	0.15	39.78	16.09

Figure 4d: Area 2 Spot 3 element distribution image and quantification from group A specimen

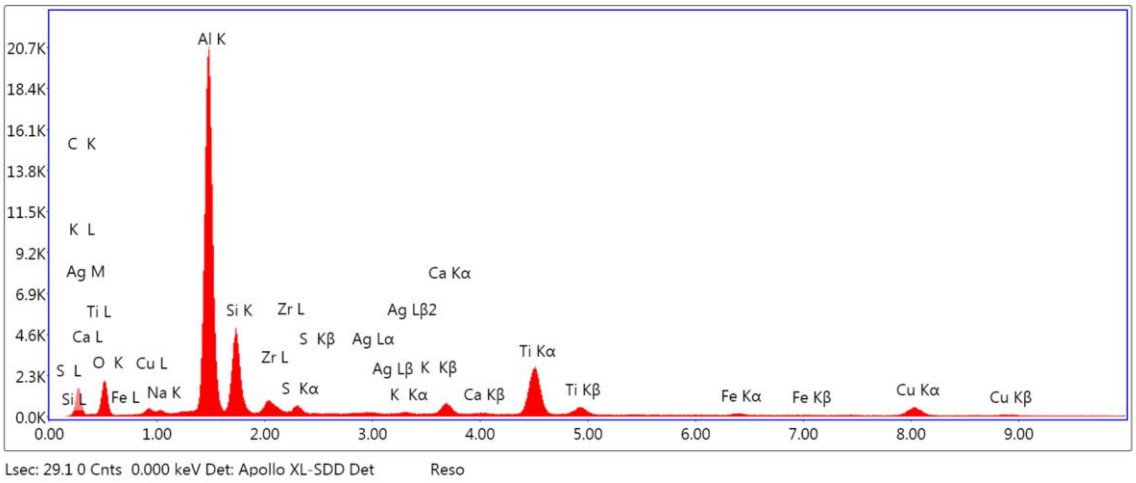

Element	Weight %	Atomic %	Net Int.	Error %
C K	34.92	51.48	341.89	9.9
O K	21.51	23.81	457.3	10.35
NaK	0.48	0.37	39.55	13.05
AlK	24.2	15.88	5983.51	5.08
SiK	7.45	4.69	1422.15	6.91
ZrL	2.24	0.44	229.07	7.31
S K	0.6	0.33	136.54	11.03
AgL	0.24	0.04	34.03	21.92
K K	0.1	0.05	28.4	19.24
CaK	0.93	0.41	234.35	4.83
TiK	4.86	1.8	1150.42	1.9
FeK	0.32	0.1	52.37	13.62
CuK	2.16	0.6	250.5	3.77

Figure 4e: Area 2 full area element distribution image and quantification from group A specimen

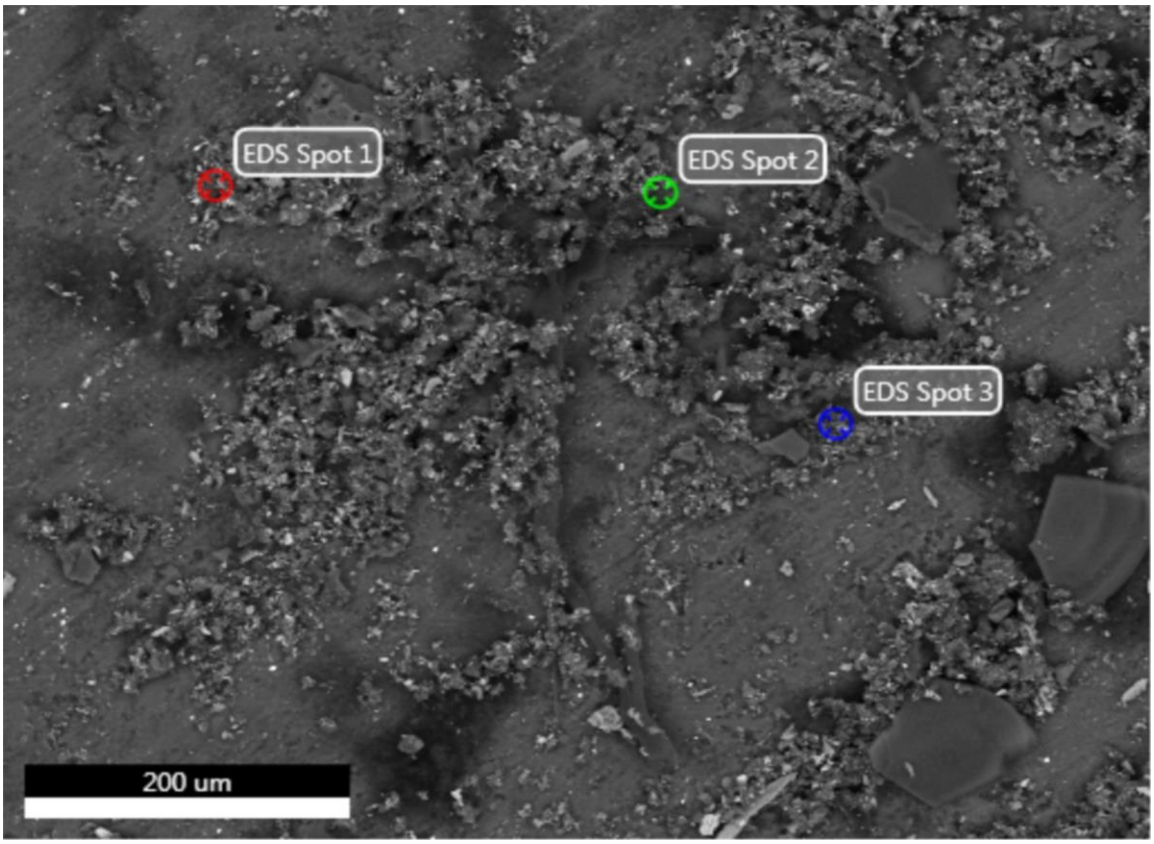

Figure 5a: Micrograph of area 3 showing areas for analysis from group A specimen

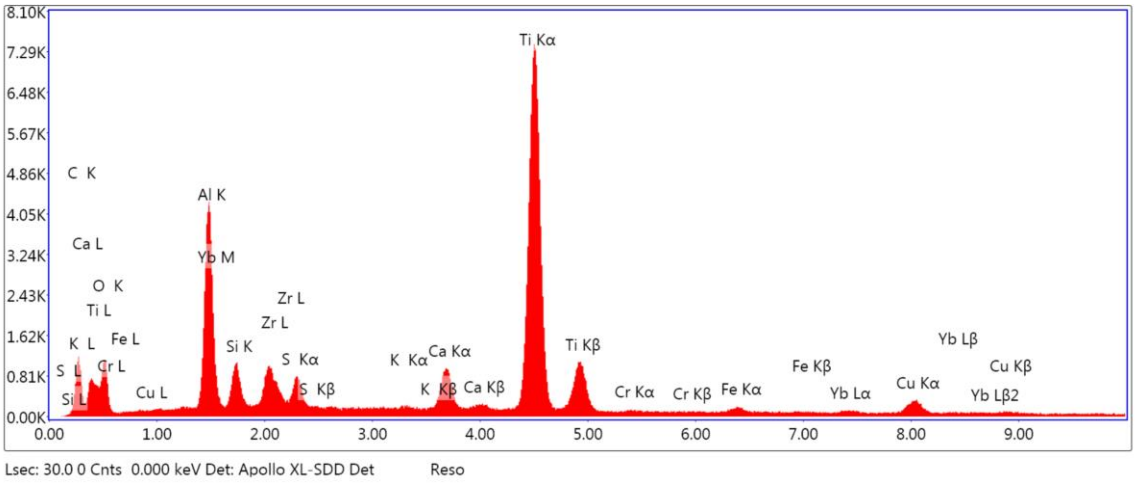

Element	Weight %	Atomic %	Net Int.	Error %
C K	28.97	47.13	229.09	9.45
O K	25.71	31.4	241.52	10.97
AlK	9.82	7.11	1069.18	6.84
SiK	2.05	1.43	249	7.86
ZrL	3.43	0.74	243.61	5.52
S K	1.32	0.8	193.18	7.17
K K	0.13	0.07	22	23.53
CaK	2.12	1.03	333.85	3.54
TiK	22.58	9.21	3075.33	1.36
CrK	0.23	0.09	22.9	34.47
FeK	0.62	0.22	54.33	14.15
YbL	0.78	0.09	30.04	31.32
CuK	2.24	0.69	143.65	5.91

Figure 5b: Area 3 spot 1 element distribution image and quantification from group A specimen

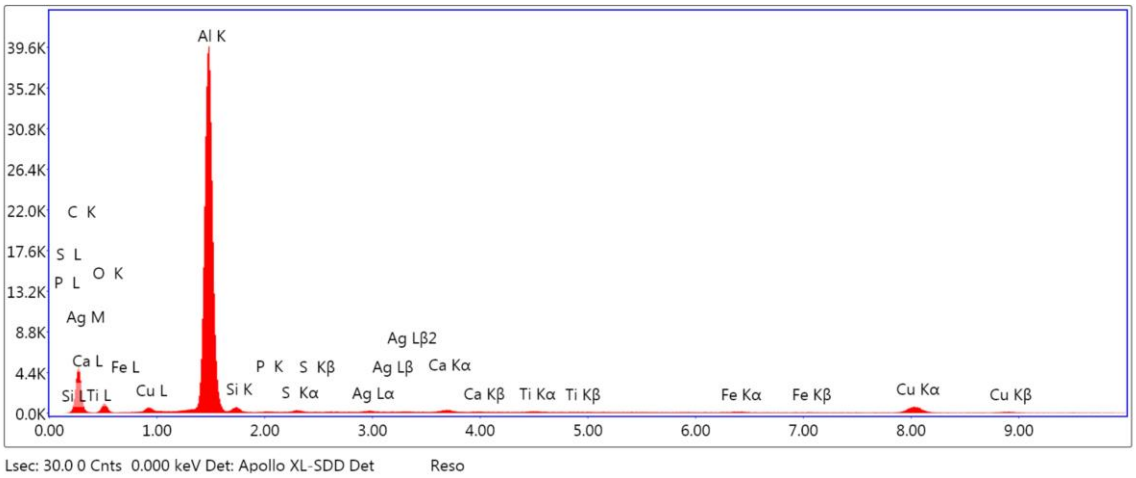

Element	Weight %	Atomic %	Net Int.	Error %
C K	59.79	74.96	1015.19	8.97
O K	8.95	8.43	226.37	10.89
AlK	28.05	15.66	11314.99	3.92
SiK	0.49	0.26	131.82	9.67
P K	0	0	0.39	71.92
S K	0.07	0.03	24.34	21.57
AgL	0.08	0.01	17.42	40.48
CaK	0.19	0.07	69.08	12.48
TiK	0.08	0.03	28.42	19.78
FeK	0.19	0.05	44.65	15.9

Figure 5c: Area 3 spot 2 element distribution image and quantification from group A specimen

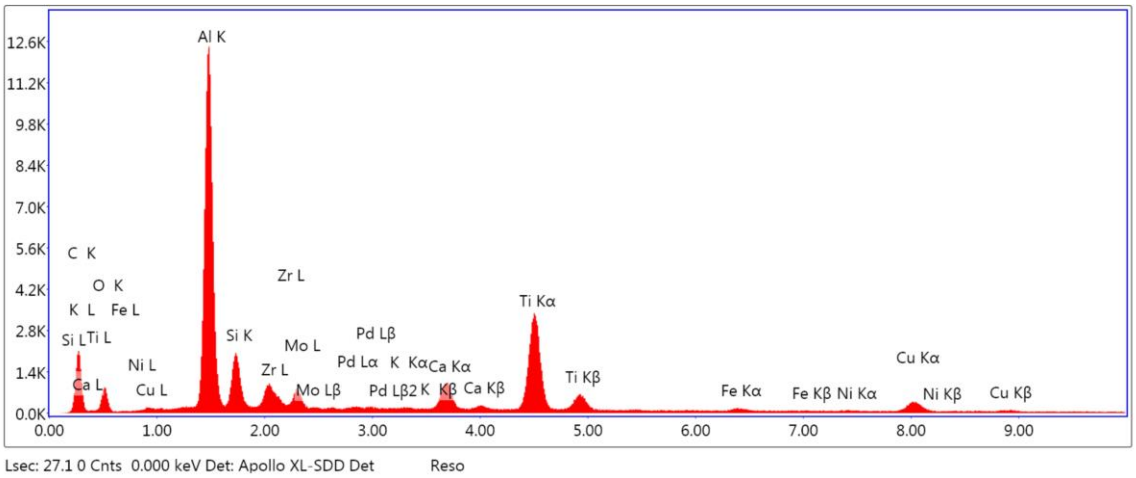

Element	Weight %	Atomic %	Net Int.	Error %
C K	46.77	65.84	476.87	9.3
O K	14.41	15.23	205.37	11.09
AlK	18.91	11.85	3798.75	5.27
SiK	3.51	2.11	609.85	6.95
ZrL	2.66	0.49	260.12	5.9
MoL	1.57	0.28	171.14	6.03
PdL	0.13	0.02	16.26	37.28
K K	0.06	0.03	14.76	53.17
CaK	1.82	0.77	394.46	3.44
TiK	7.6	2.68	1501.3	1.73
FeK	0.37	0.11	48.82	15.72
NiK	0.18	0.05	20.38	27.48
CuK	2.01	0.53	192.15	5.01

Figure 5d: Area 3 spot 3 element distribution image and quantification from group A specimen

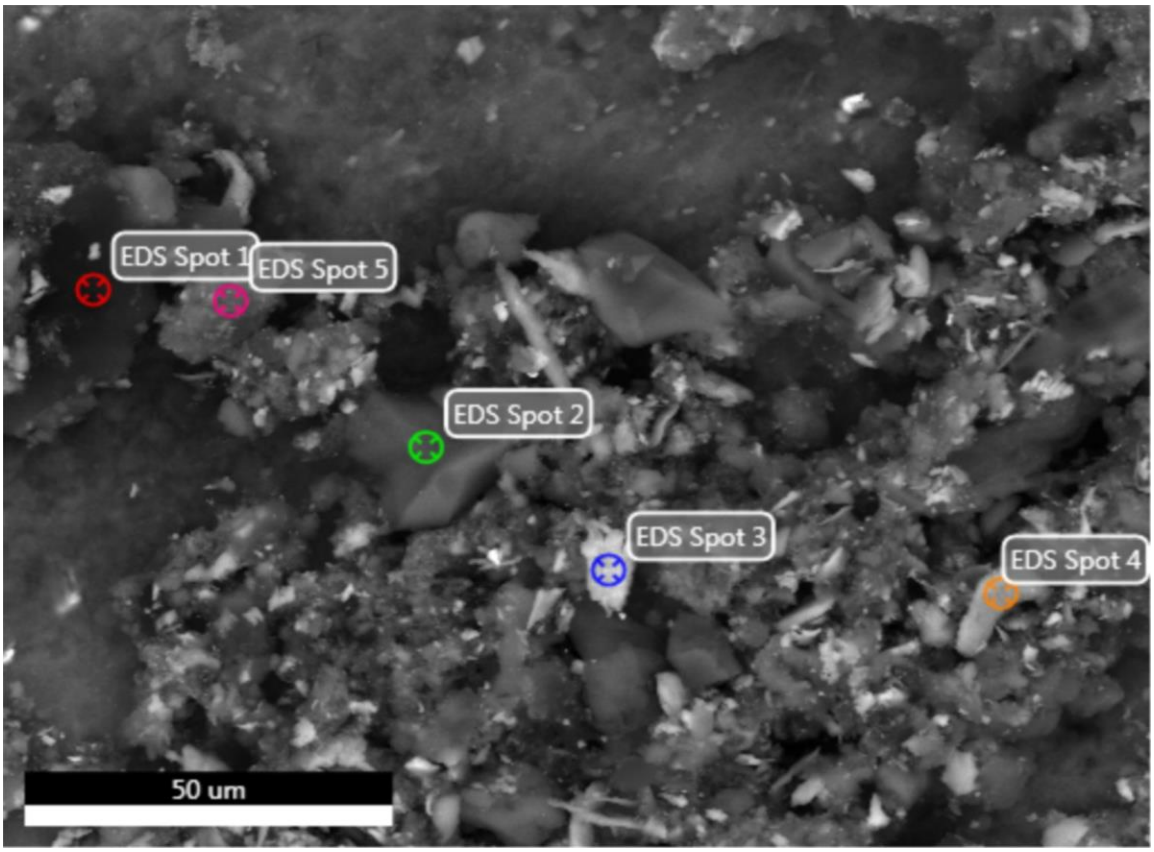

Figure 6a: Micrograph of area 4 showing areas for analysis from group A specimen

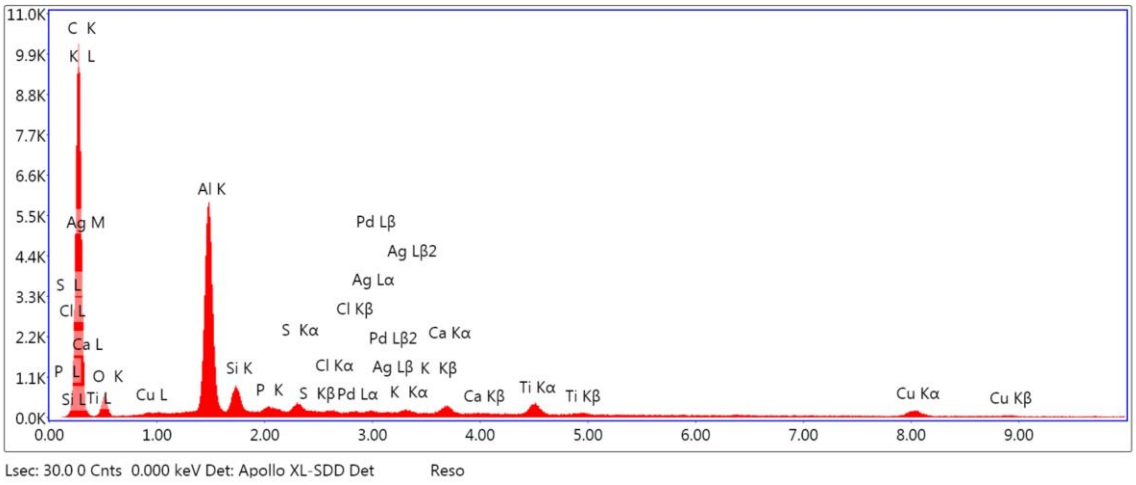

Element	Weight %	Atomic %	Net Int.	Error %
C K	81.25	88.22	1971.19	6.2
O K	9.6	7.82	134.84	11.41
AlK	6.2	3	1603.84	4.4
SiK	0.71	0.33	200.58	5.97
P K	0.15	0.06	42.25	12.14
S K	0.24	0.1	77.12	9
ClK	0.05	0.02	15.6	20.65
PdL	0.04	0.01	6.95	60.03
AgL	0.09	0.01	13.88	40.49
K K	0.11	0.04	32.95	14.3
CaK	0.31	0.1	80.52	10.53
TiK	0.51	0.14	119.29	6.49
CuK	0.74	0.15	79.12	9.66

Figure 6b: Area 4 spot 1 element distribution image and quantification from group A specimen

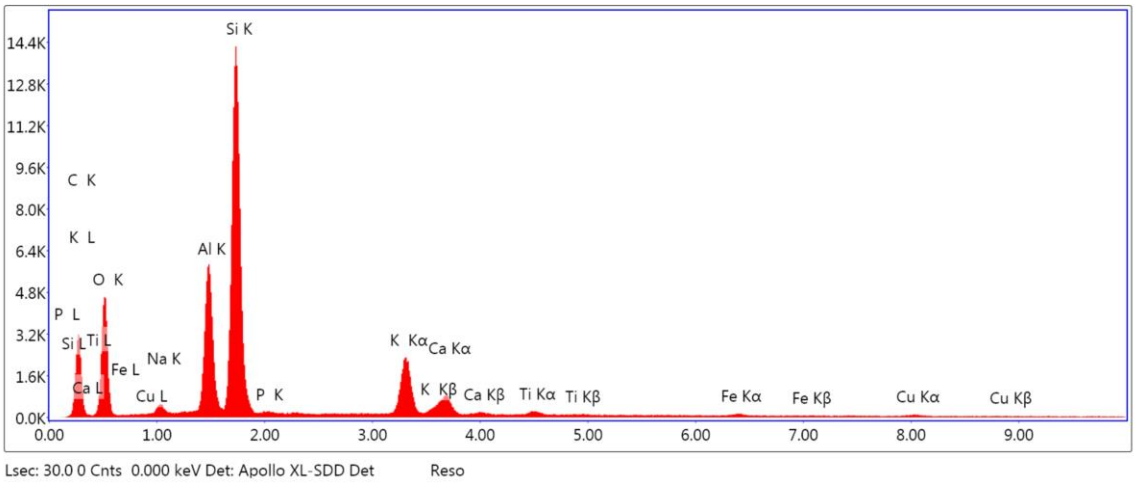

Element	Weight %	Atomic %	Net Int.	Error %
C K	39.19	50.97	618.96	8.99
O K	37.18	36.31	1058.14	9.76
NaK	1.1	0.75	98.28	10.36
AlK	5.83	3.38	1629.8	5.58
SiK	12.74	7.08	4114.24	4.73
P K	0.1	0.05	25.98	21.11
K K	2.35	0.94	813.14	2.35
CaK	0.89	0.35	275.91	3.65
TiK	0.22	0.07	62.1	11.25
FeK	0.18	0.05	34.87	16.12
CuK	0.22	0.05	29.89	18.46

Figure 6c: Area 4 spot 2 element distribution image and quantification from group A specimen

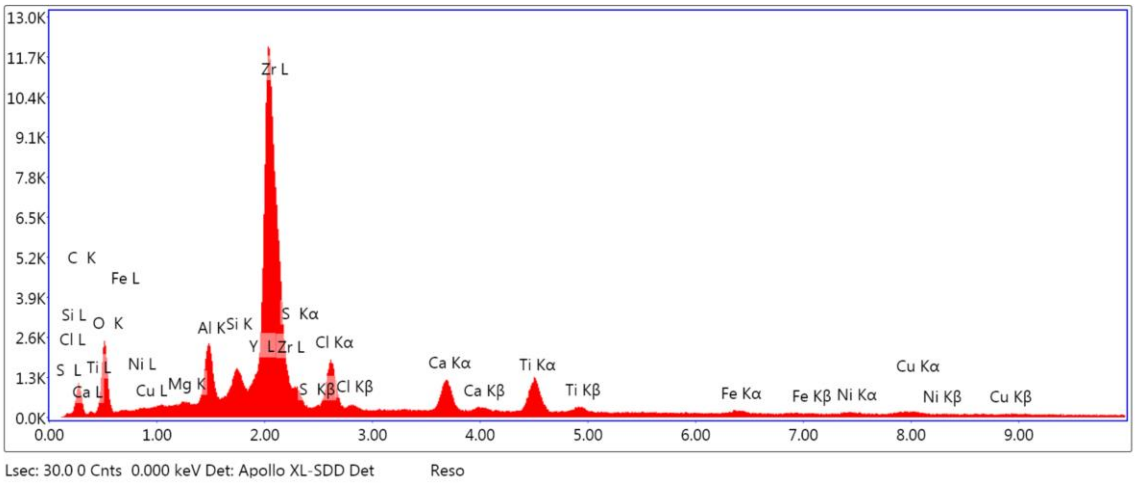

Element	Weight %	Atomic %	Net Int.	Error %
C K	23.13	41.1	188.91	10.82
O K	31.15	41.54	571.15	10.22
MgK	1.12	0.98	142.82	9.64
AlK	3.56	2.82	653.84	6.96
SiK	1.57	1.2	369.09	6.9
Y L	2.27	0.54	272.97	4.74
ZrL	26.36	6.17	3374.93	1.06
S K	1.28	0.85	213.73	12.1
ClK	3.31	1.99	578.25	6.73
CaK	2.15	1.14	428.6	5.09
TiK	2.41	1.07	478.83	3.87
FeK	0.51	0.19	74.62	12.21
NiK	0.4	0.15	50.45	15.02
CuK	0.78	0.26	84.28	12

Figure 6d: Area 4 spot 3 element distribution image and quantification from group A specimen

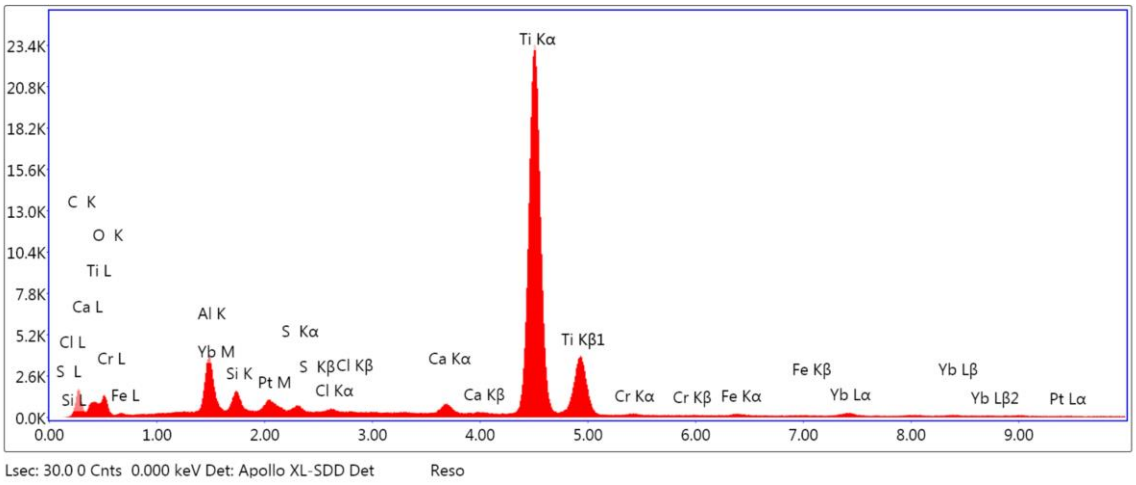

Element	Weight %	Atomic %	Net Int.	Error %
C K	22.14	41.54	367.15	8.47
O K	21.96	30.93	285.21	11.12
AlK	4.74	3.96	794.89	7.47
SiK	1.94	1.56	405.85	7.56
PtM	2.45	0.28	236.81	10.05
S K	0.54	0.38	141.42	10.87
ClK	0.32	0.21	88.52	11.67
CaK	0.93	0.52	266.78	4.6
TiK	42.75	20.11	9960.4	1.08
CrK	0.4	0.18	62.84	21.25
FeK	0.38	0.15	52.59	19.06
YbL	1.45	0.19	92.44	16.86

Figure 6e: Area 4 spot 4 element distribution image and quantification from group A specimen

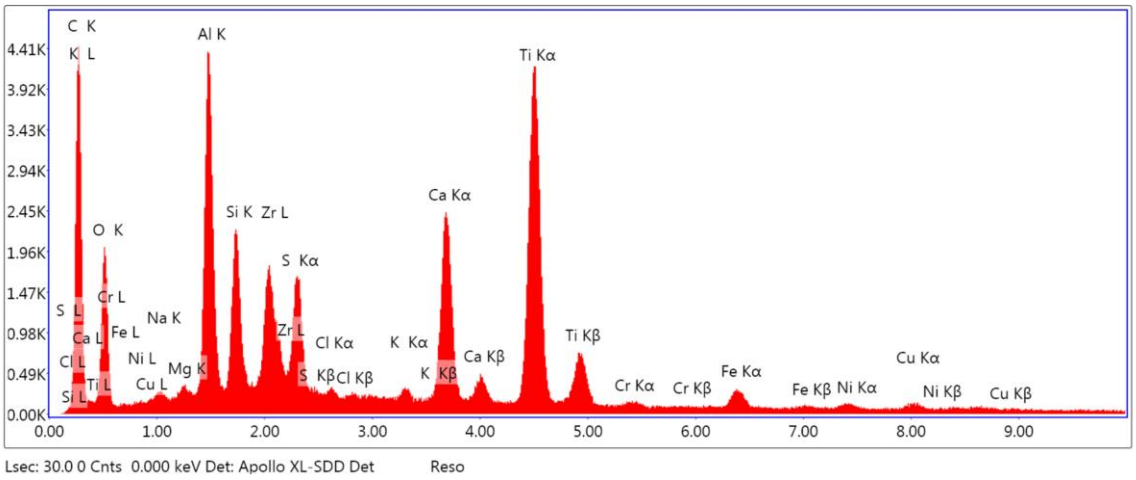

Element	Weight %	Atomic %	Net Int.	Error %
C K	50.36	65.53	882.16	8.14
O K	25.01	24.43	449.03	10.45
NaK	0.56	0.38	40.61	12.31
MgK	0.25	0.16	38.74	11.2
AlK	5.18	3	1190.65	6.04
SiK	2.14	1.19	590.92	5.71
ZrL	3.15	0.54	477.74	3.75
S K	1.63	0.79	496.23	4.28
ClK	0.14	0.06	41.33	15.18
K K	0.2	0.08	64.12	9.79
CaK	3.15	1.23	895.28	1.76
TiK	6.85	2.23	1712.86	1.33
CrK	0.16	0.05	31.78	16.81
FeK	0.65	0.18	108.05	8.2
NiK	0.24	0.06	33.61	17.55
CuK	0.33	0.08	39.24	15.87

Figure 6f: Area 4 spot 5 element distribution image and quantification from group A specimen

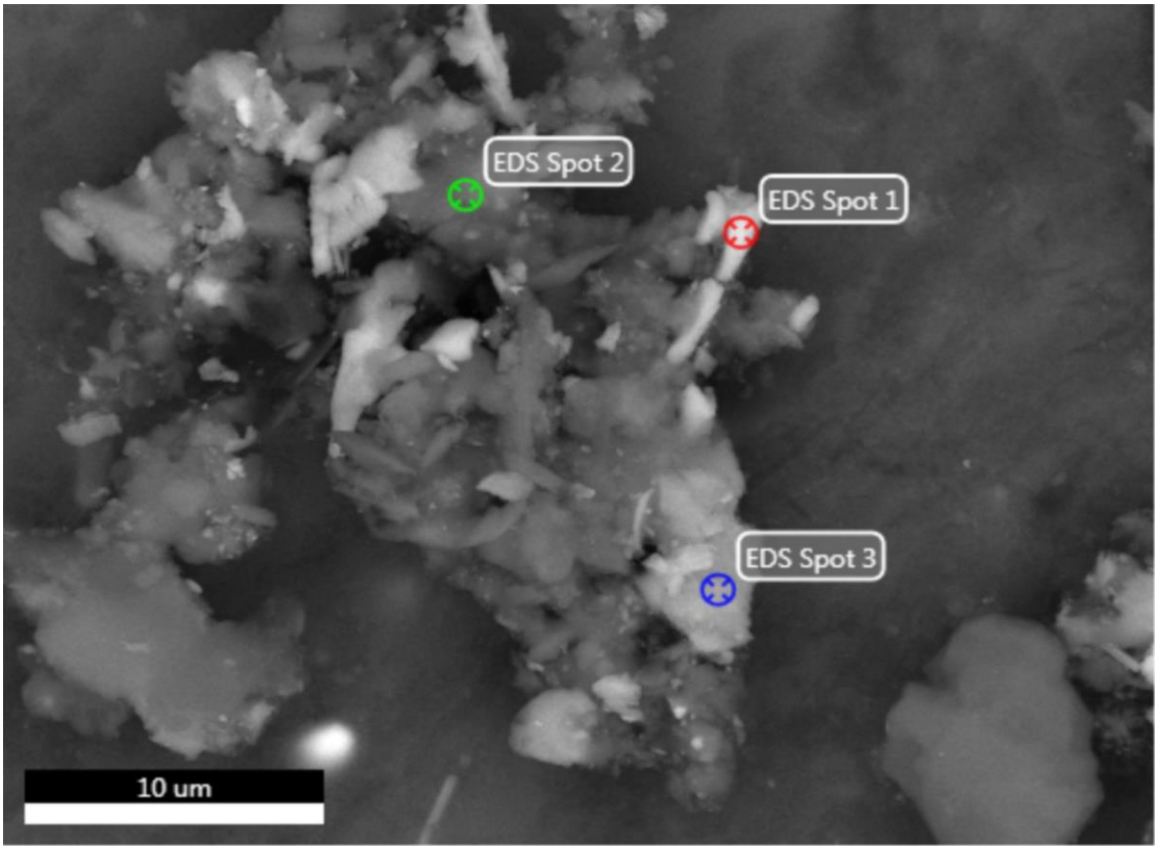

Figure 7a: Micrograph of area 5 showing areas for analysis from group A specimen

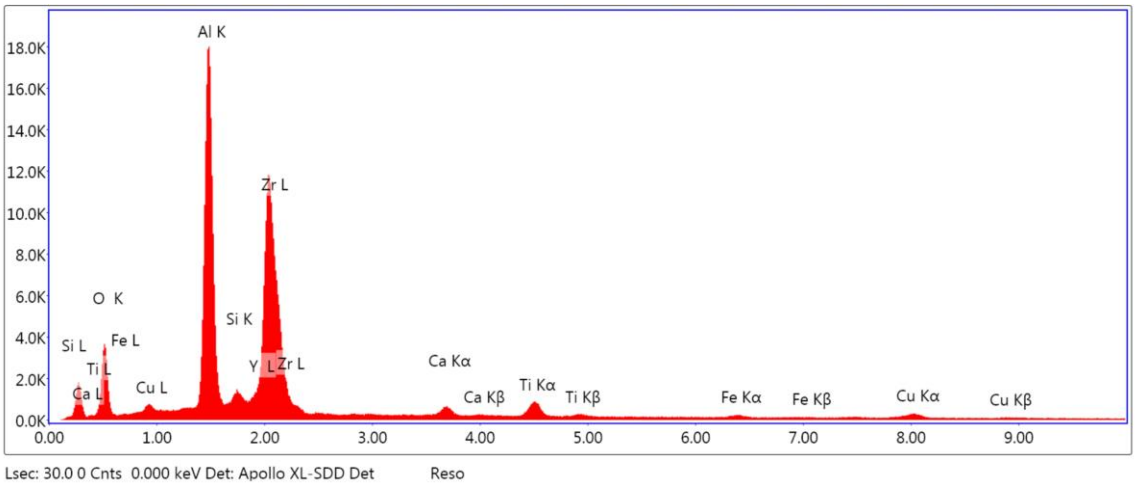

Element	Weight %	Atomic %	Net Int.	Error %
O K	33.71	58.99	849.26	9.78
AlK	24.86	25.8	5231.66	6.03
SiK	2.04	2.04	360.58	8.4
Y L	3.04	0.96	284.68	6.81
ZrL	32.25	9.9	3286.15	3.65
CaK	1.04	0.73	205.23	8.11
TiK	1.54	0.9	316	5.13
FeK	0.38	0.19	58.94	14.97
CuK	1.14	0.5	133.96	7.97

Figure 7b: Area 5 spot 1 element distribution image and quantification from group A specimen

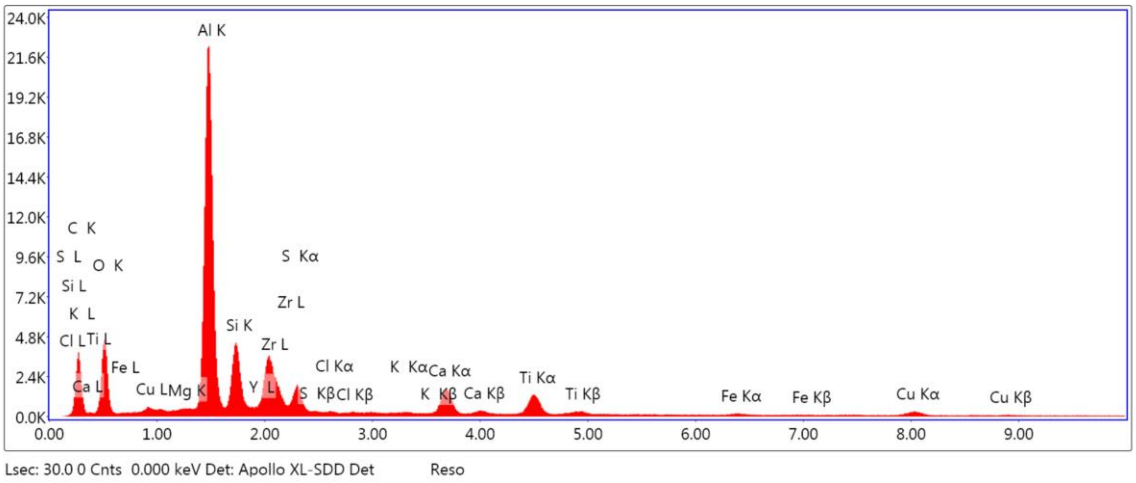

Element	Weight %	Atomic %	Net Int.	Error %
C K	38.35	52.97	696.43	9.31
O K	30.11	31.23	1063.17	9.87
MgK	0.43	0.3	116.41	8.95
AlK	16.68	10.26	6375.04	5.22
SiK	3.65	2.15	1267.31	6.36
Y L	0.56	0.1	97.92	8.31
ZrL	5	0.91	959.07	3
S K	1.34	0.69	516.91	5.49
ClK	0.09	0.04	34.64	16.48
K K	0.1	0.04	43.88	13.6
CaK	1.46	0.6	589.85	2.85
TiK	1.35	0.47	510.11	2.47
FeK	0.19	0.06	50.06	13.75
CuK	0.69	0.18	128.47	7.38

Figure 7c: Area 5 spot 2 element distribution image and quantification from group A specimen

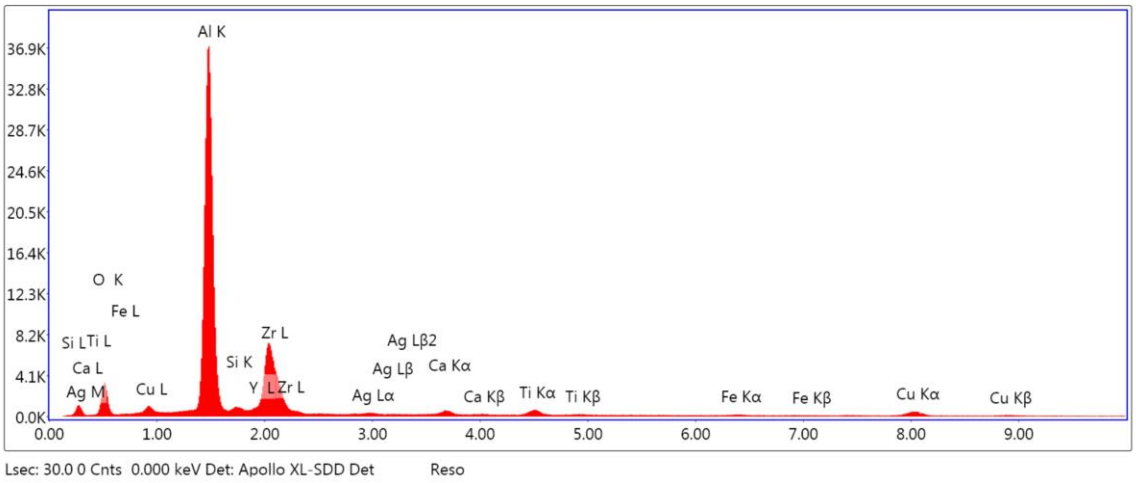

Element	Weight %	Atomic %	Net Int.	Error %
O K	26.53	45.36	777.77	9.69
AlK	42.71	43.3	10798.57	5.35
SiK	1.86	1.81	279.23	9.36
Y L	2.29	0.7	187.94	8.43
ZrL	21.86	6.56	1997.71	4.94
AgL	0.79	0.2	86.6	13.19
CaK	0.79	0.54	171.44	8.37
TiK	0.99	0.57	221.76	5.77
FeK	0.3	0.15	51.65	15.83
CuK	1.88	0.81	235.65	4.44

Figure 7d: Area 5 spot 3 element distribution image and quantification from group A specimen

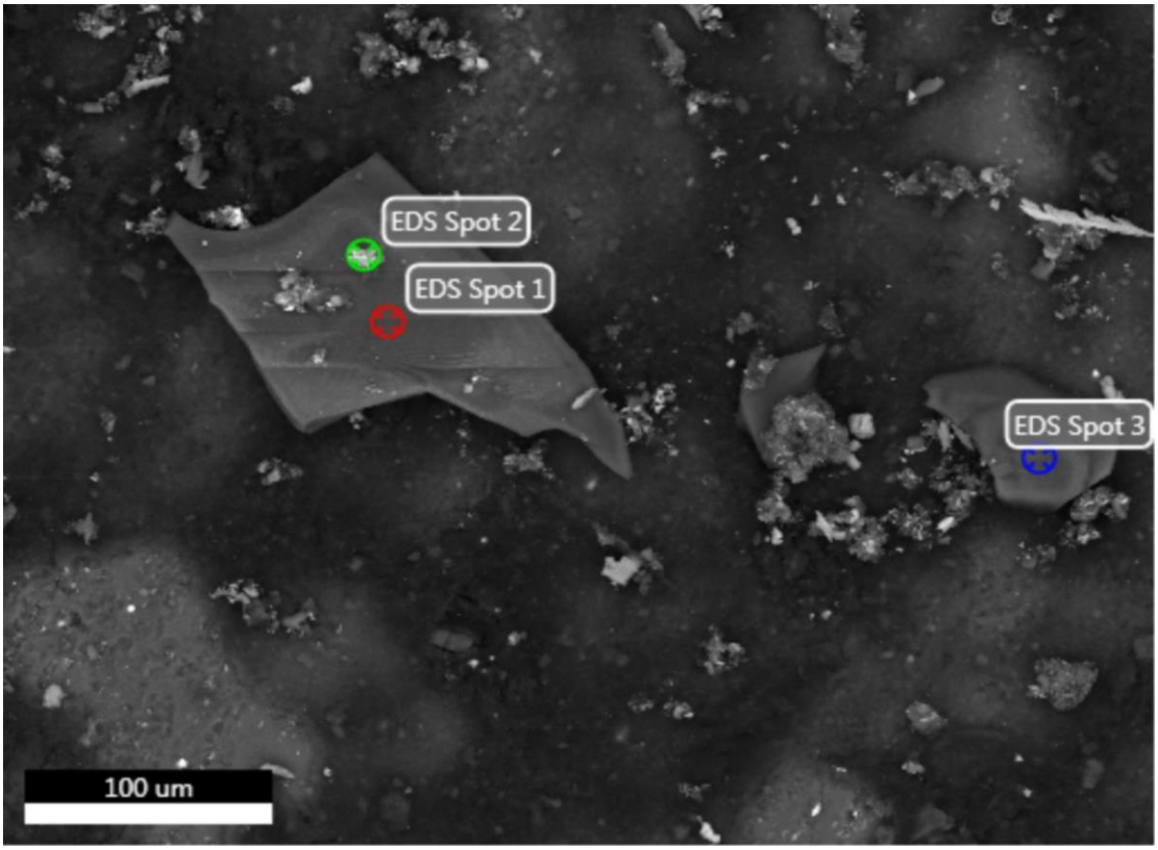

Figure 8a: Micrograph of area 6 showing areas for analysis from group A specimen

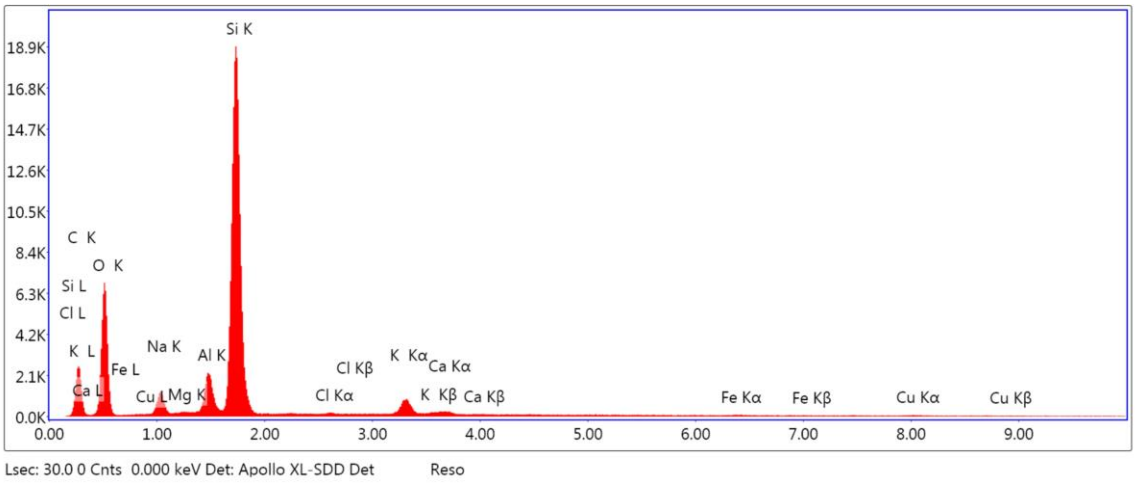

Element	Weight %	Atomic %	Net Int.	Error %
C K	32.89	43.3	492.71	9.26
O K	43.87	43.36	1513.43	9.38
NaK	3.33	2.29	293.44	9.62
MgK	0.12	0.08	21.94	37.23
AlK	2.25	1.32	595.84	6.45
SiK	16.31	9.18	5513.5	4.5
ClK	0.03	0.01	8.71	59.98
K K	0.81	0.33	280.76	4.12
CaK	0.18	0.07	55.08	13.77
FeK	0.08	0.02	15.3	41.14
CuK	0.14	0.03	19.05	24.87

Figure 8b: Area 6 spot 1 element distribution image and quantification from group A specimen

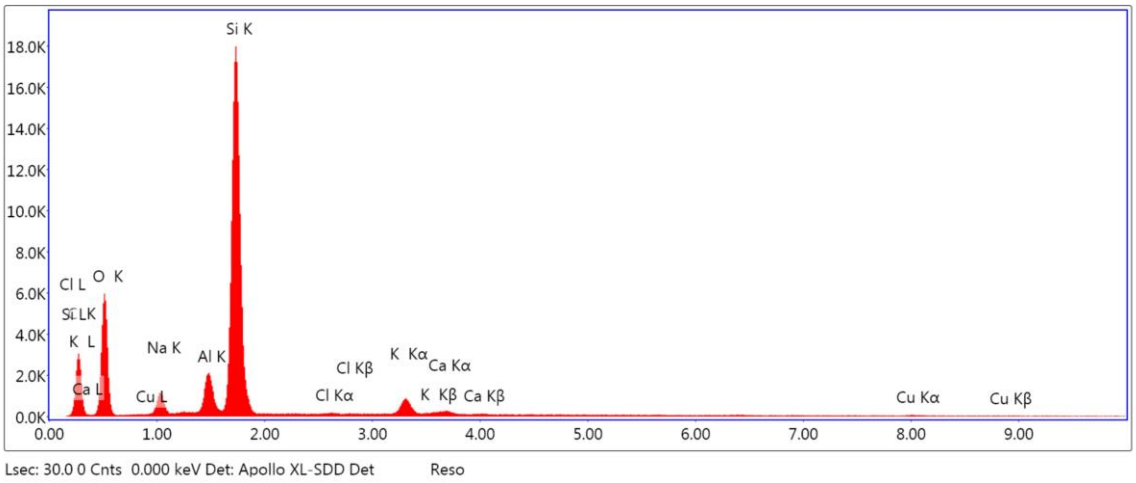

Element	Weight %	Atomic %	Net Int.	Error %
C K	37.82	48.48	617.84	8.94
O K	41.51	39.95	1349.5	9.53
NaK	2.88	1.93	261.87	9.57
AlK	2	1.14	551.87	6.32
SiK	14.85	8.14	5229.24	4.33
ClK	0.01	0	1.94	60.27
K K	0.72	0.28	255.68	4
CaK	0.16	0.06	50.66	13.6
CuK	0.05	0.01	7.5	57.95

Figure 8c: Area 6 spot 2 element distribution image and quantification from group A specimen

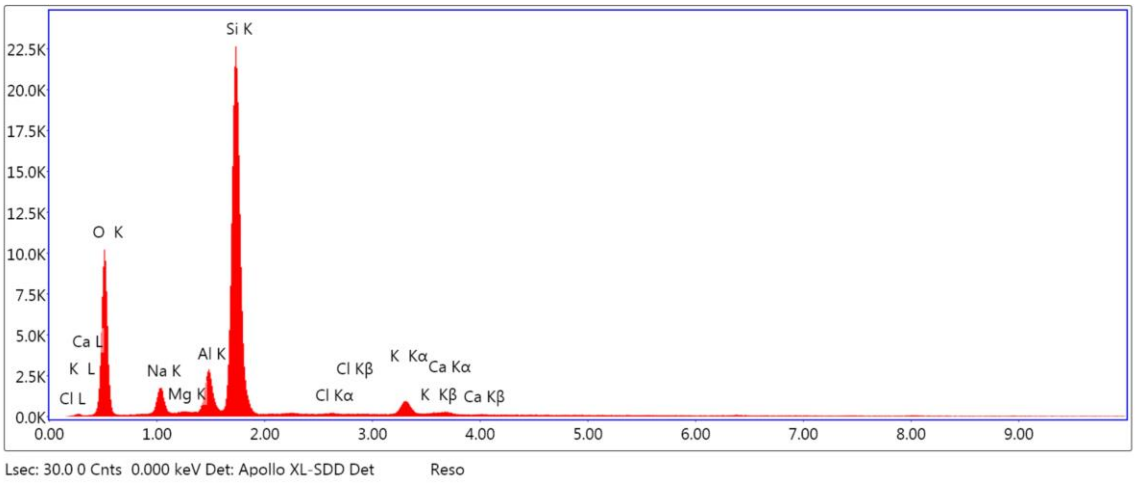

Element	Weight %	Atomic %	Net Int.	Error %
O K	53.71	66.42	2253.75	8.05
NaK	7.45	6.41	468.25	9.36
MgK	0.59	0.48	67.21	10.1
AlK	4.6	3.37	775.08	6.79
SiK	31.68	22.32	6556.71	5.31
ClK	0.18	0.1	33.13	19.26
K K	1.48	0.75	313.97	5.03
CaK	0.32	0.16	63.1	12.96

Figure 8d: Area 6 spot 3 element distribution image and quantification from group A specimen

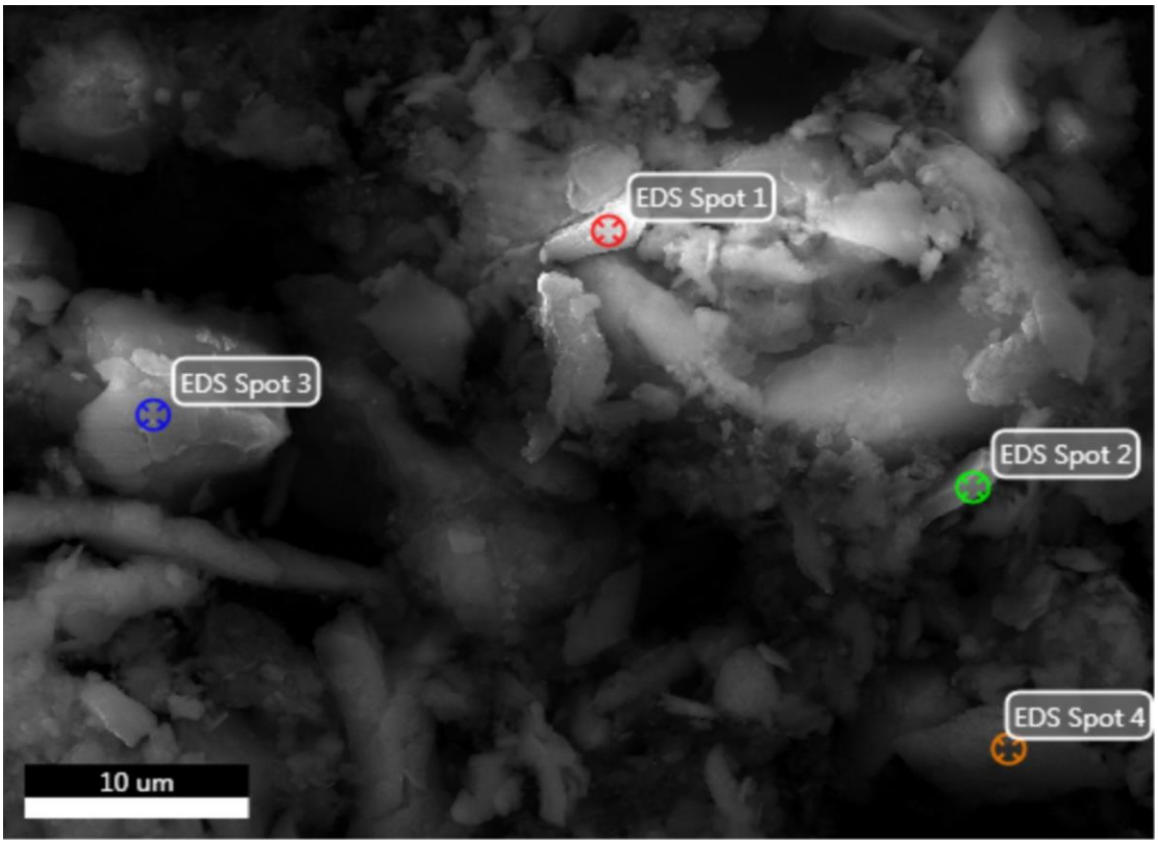

Figure 9a: Micrograph of area 7 showing areas for analysis from group A specimen

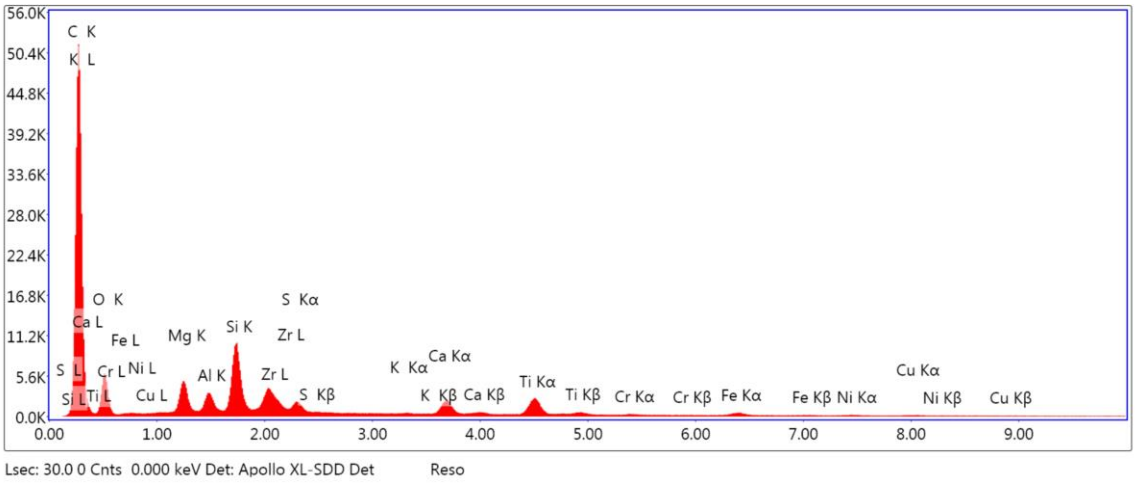

Element	Weight %	Atomic %	Net Int.	Error %
C K	74.81	82.49	10265.04	5.73
O K	17.71	14.66	1435.62	10.12
MgK	1.47	0.8	1329.89	6.72
AlK	0.7	0.35	878.63	5.44
SiK	1.82	0.86	2939.25	3.57
ZrL	1.37	0.2	1145.28	4.33
S K	0.32	0.13	540.88	3.01
K K	0.04	0.01	65.32	10.87
CaK	0.54	0.18	763.45	2.27
TiK	0.8	0.22	1009.11	2.29
CrK	0.08	0.02	76.2	12.24
FeK	0.23	0.05	187.66	6.49
NiK	0.06	0.01	41.97	19.96
CuK	0.06	0.01	36.23	20.8

Figure 9b: Area 7 spot 1 element distribution image and quantification from group A specimen

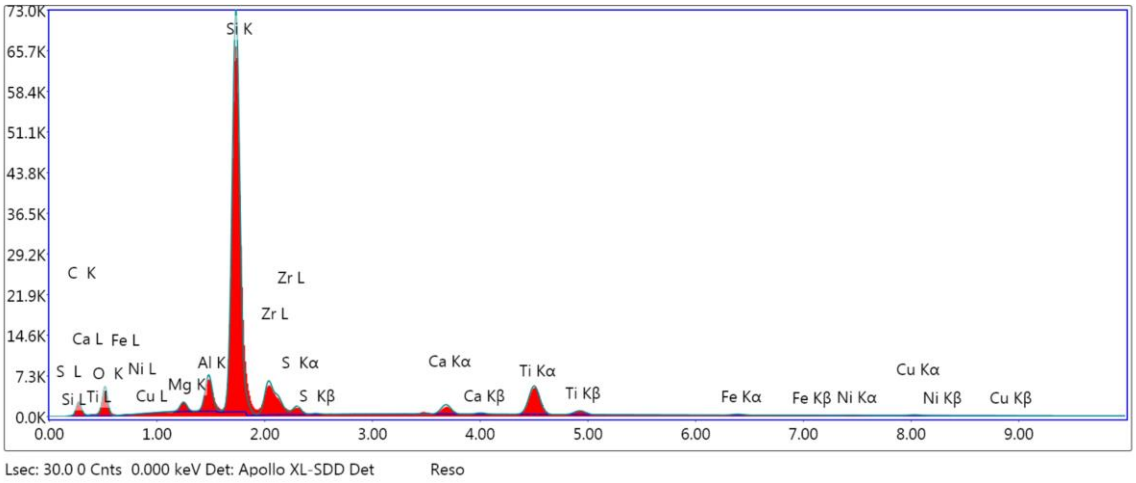

Element	Weight %	Atomic %	Net Int.	Error %
C K	25.71	41.75	430.45	10.42
O K	22.97	28	1071.78	9.91
MgK	1.44	1.15	564.81	7.38
AlK	3.39	2.45	1836.59	5.53
SiK	31.3	21.74	20184.65	4.16
ZrL	7.87	1.68	1579.91	4.92
S K	0.94	0.57	379.81	8.72
CaK	1.31	0.64	666.87	4.12
TiK	4.33	1.76	2126	2.21
FeK	0.31	0.11	106.4	11.59
NiK	0.14	0.05	40.35	19.41
CuK	0.3	0.09	76.82	13.27

Figure 9c: Area 7 spot 2 element distribution image and quantification from group A specimen

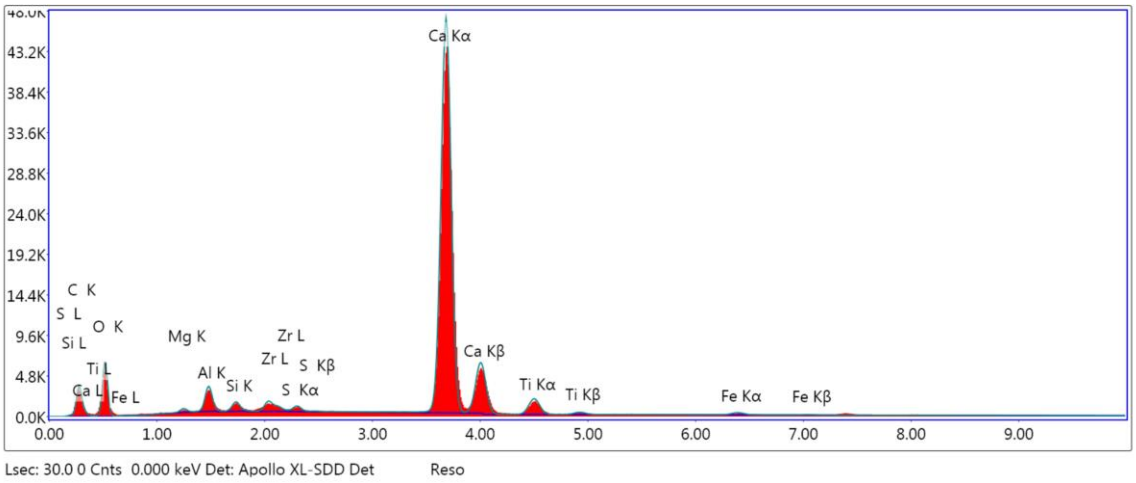

Element	Weight %	Atomic %	Net Int.	Error %
C K	13.64	23.02	489.87	7.89
O K	43.21	54.75	1280.04	10.14
MgK	0.56	0.46	117.71	26.65
AlK	2.42	1.82	776.75	7.61
SiK	0.68	0.49	294.44	8.1
ZrL	1.26	0.28	333.64	4.91
S K	0.33	0.21	182.92	9.2
CaK	35.6	18.01	17445.37	0.88
TiK	1.92	0.81	679.38	4.26
FeK	0.39	0.14	104.68	13.6

Figure 9d: Area 7 spot 3 element distribution image and quantification from group A specimen

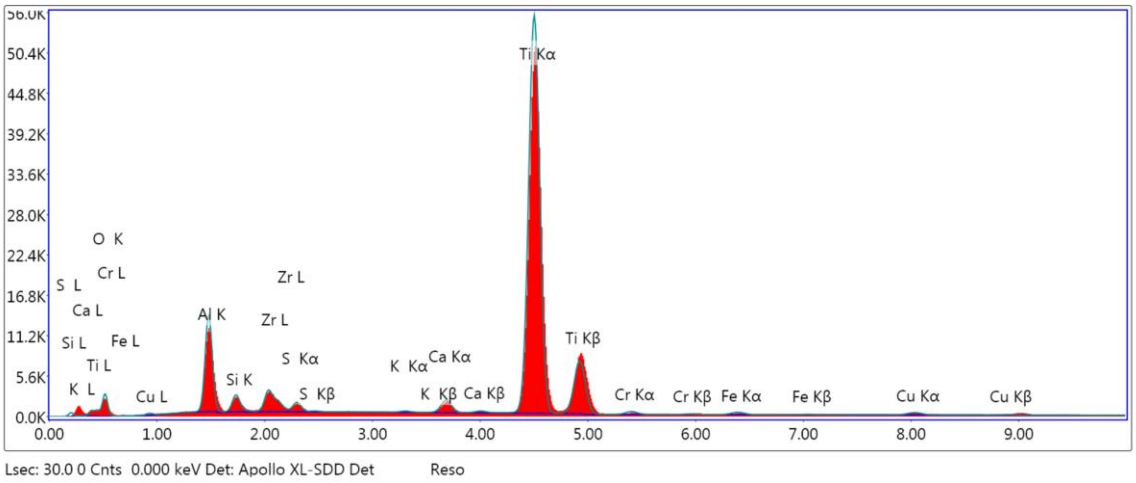

Element	Weight %	Atomic %	Net Int.	Error %
O K	25.11	47.19	614.79	10.57
AlK	12.15	13.54	3506.57	7.27
SiK	1.98	2.12	655.09	7.97
ZrL	4.15	1.37	850.95	5.1
S K	0.9	0.85	384.98	8.08
K K	0.12	0.09	63.18	16.24
CaK	1.23	0.92	639.8	3.61
TiK	52.57	33	22472.6	1.29
CrK	0.47	0.27	130.11	12.81
FeK	0.5	0.27	127.35	12.84
CuK	0.81	0.38	158.42	11.22

Figure 9e: Area 7 spot 4 element distribution image and quantification from group A specimen

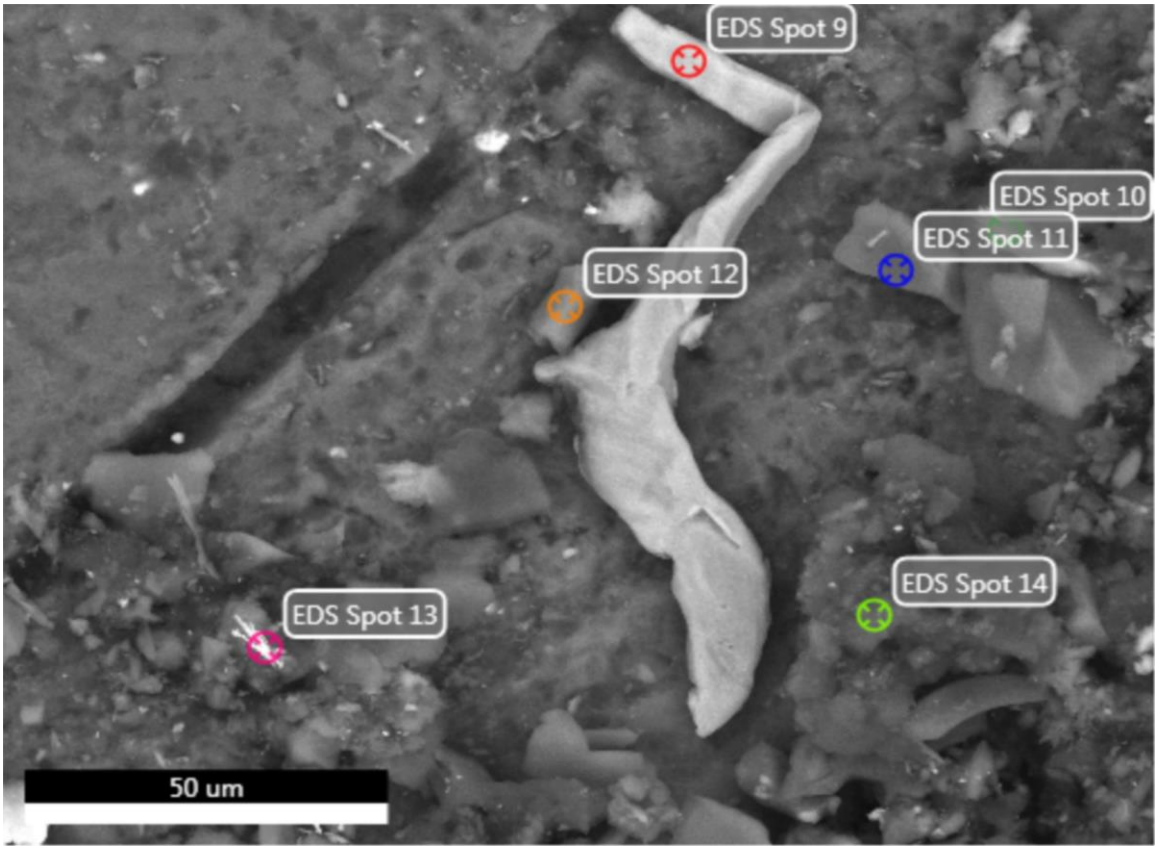

Figure 10a: Micrograph of area 8 showing areas for analysis from group B specimen

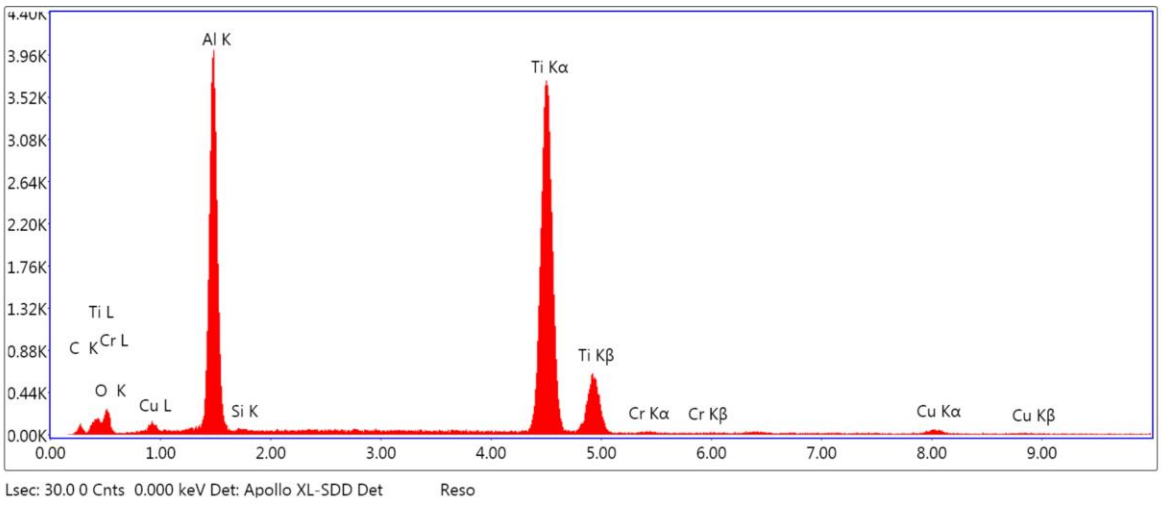

Element	Weight %	Atomic %	Net Int.	Error %
C K	11.16	23.29	20.39	13.34
O K	16.86	26.41	50.79	12.71
CuL	4.48	1.77	24.3	12.72
AlK	32.13	29.85	1129.95	6.79
SiK	0.53	0.47	14.28	29.76
TiK	34.58	18.09	1528.89	1.59
CrK	0.26	0.12	7.9	37.17

Figure 10b: Area 8 spot 9 element distribution image and quantification from group B specimen

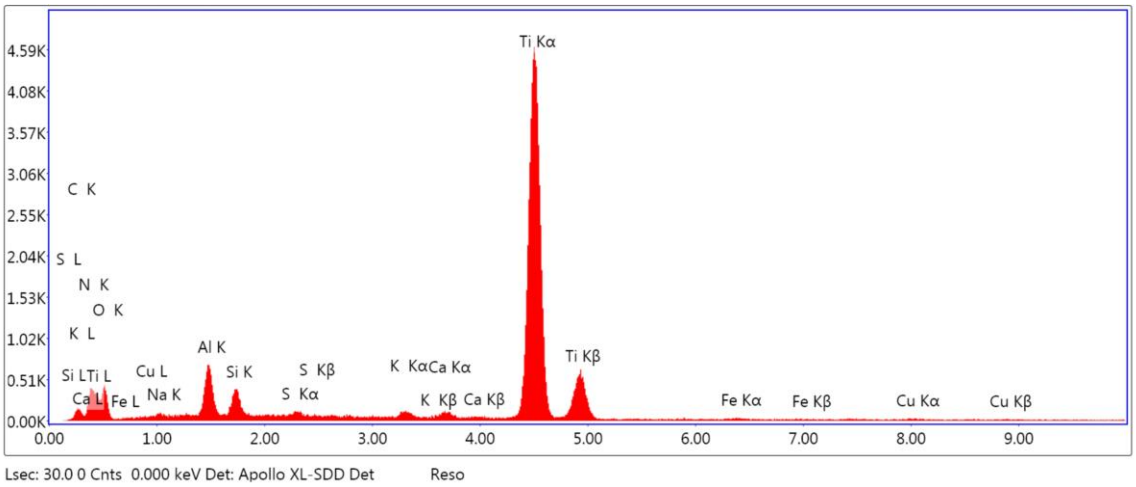

Element	Weight %	Atomic %	Net Int.	Error %
C K	9.66	17.63	30.95	11.73
N K	8.15	12.74	25.36	14.24
O K	30.2	41.37	88.22	11.96
NaK	2.88	2.75	29.61	15.35
AlK	5.81	4.72	191.69	8.62
SiK	2.52	1.97	106.24	8.51
S K	0.53	0.36	29.4	12.1
K K	0.5	0.28	32.36	11.54
CaK	0.49	0.27	29.95	12.68
TiK	38.79	17.75	1908.51	1.17
FeK	0.24	0.09	7.09	43.45
CuK	0.22	0.08	4.91	59.34

Figure 10c: Area 8 spot 10 element distribution image and quantification from group B specimen

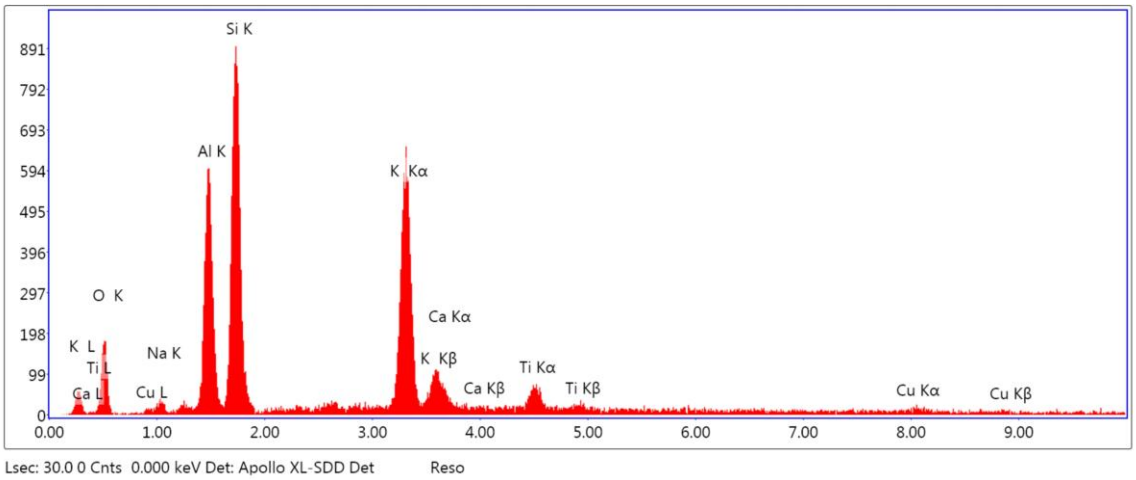

Element	Weight %	Atomic %	Net Int.	Error %
O K	34.89	51.15	38.49	12.73
NaK	0.8	0.81	2.72	48.58
AlK	15.03	13.07	158.04	7.17
SiK	25.49	21.28	257.01	7.14
K K	18.44	11.06	217.67	4.43
CaK	1.57	0.92	14.79	20.9
TiK	2.59	1.27	24.74	14.89
CuK	1.19	0.44	6.22	37.66

Figure 10d: Area 8 spot 11 element distribution image and quantification from group B specimen

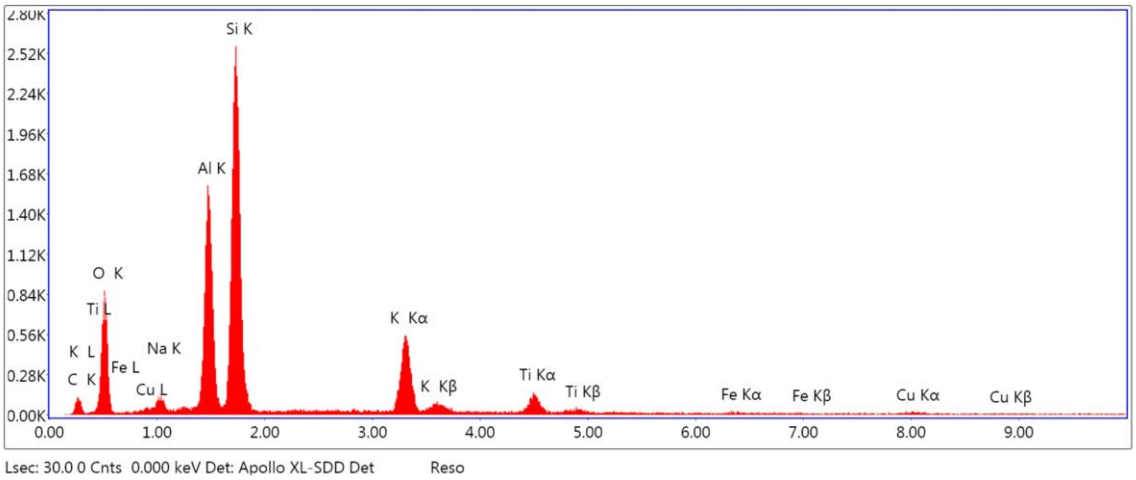

Element	Weight %	Atomic %	Net Int.	Error %
C K	16.06	24.79	22.14	13.79
O K	41.19	47.74	189.23	10.29
NaK	2.65	2.13	30.86	12.27
AlK	12.44	8.55	432.31	6.35
SiK	20.91	13.81	731.03	6.21
K K	4.74	2.25	192.24	4.44
TiK	1.45	0.56	51.02	7.71
FeK	0.17	0.06	4.06	59.72
CuK	0.4	0.12	7.12	30.7

Figure 10e: Area 8 spot 12 element distribution image and quantification from group B specimen

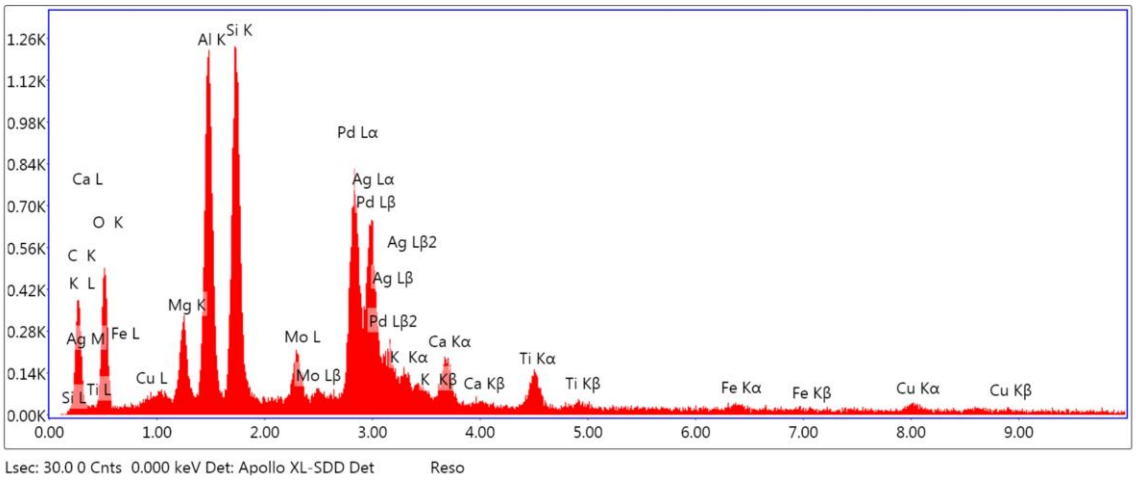

Element	Weight %	Atomic %	Net Int.	Error %
C K	28.66	45.38	68.86	10.78
O K	29.11	34.6	111.71	11.24
MgK	3.1	2.42	79.01	10.04
AlK	9.68	6.82	334.75	7.34
SiK	8.98	6.08	348.46	7
MoL	1.93	0.38	44.89	8.14
PdL	9.51	1.7	243.67	3.87
AgL	4.78	0.84	122.57	6.43
K K	0.58	0.28	26.37	16.08
CaK	1.48	0.7	57.72	9.81
TiK	1.16	0.46	44.55	13.04
FeK	0.36	0.12	10.14	27.55
CuK	0.68	0.2	13.91	20.96

Figure 10f: Area 8 spot 13 element distribution image and quantification from group B specimen

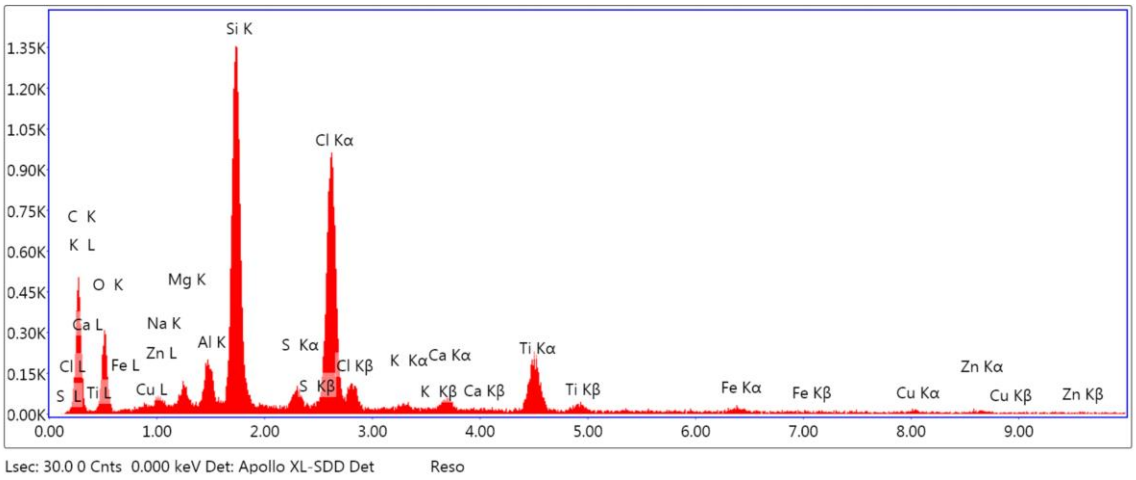

Element	Weight %	Atomic %	Net Int.	Error %
C K	54.63	67.86	95.45	10.44
O K	23.62	22.03	62.63	12.01
NaK	0	0	0.03	29.1
MgK	0.91	0.56	23.09	12.1
AlK	1.37	0.76	49.27	8.5
SiK	8.65	4.59	397.49	4.54
S K	0.49	0.23	22.33	12.69
ClK	6.9	2.9	314.02	3.02
K K	0.2	0.08	8.28	23.01
CaK	0.39	0.15	15.11	16.91
TiK	2.18	0.68	77.52	4.71
FeK	0.28	0.08	6.76	30.82
CuK	0.18	0.04	3.1	61.51
ZnK	0.19	0.04	2.81	62.14

Figure 10g: Area 8 spot 14 element distribution image and quantification from group B specimen

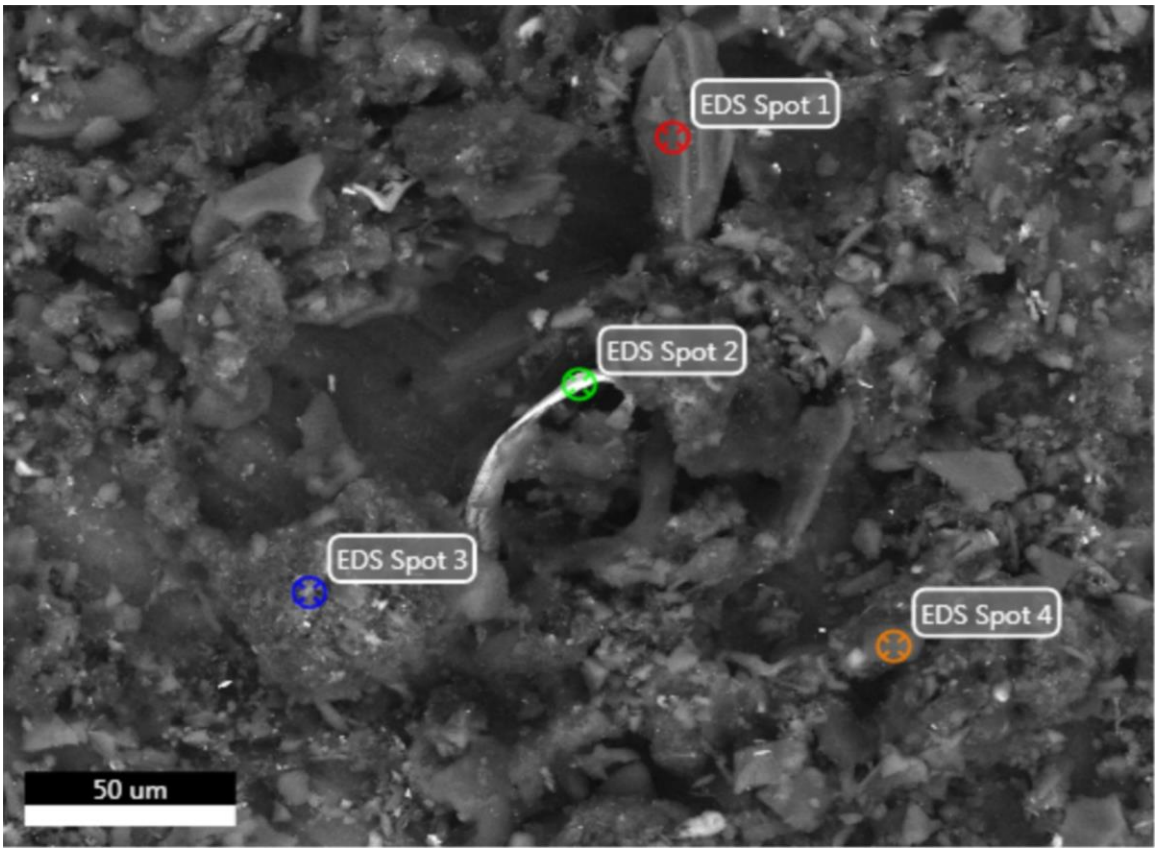

Figure 11a: Micrograph of area 9 showing areas for analysis from group B specimen

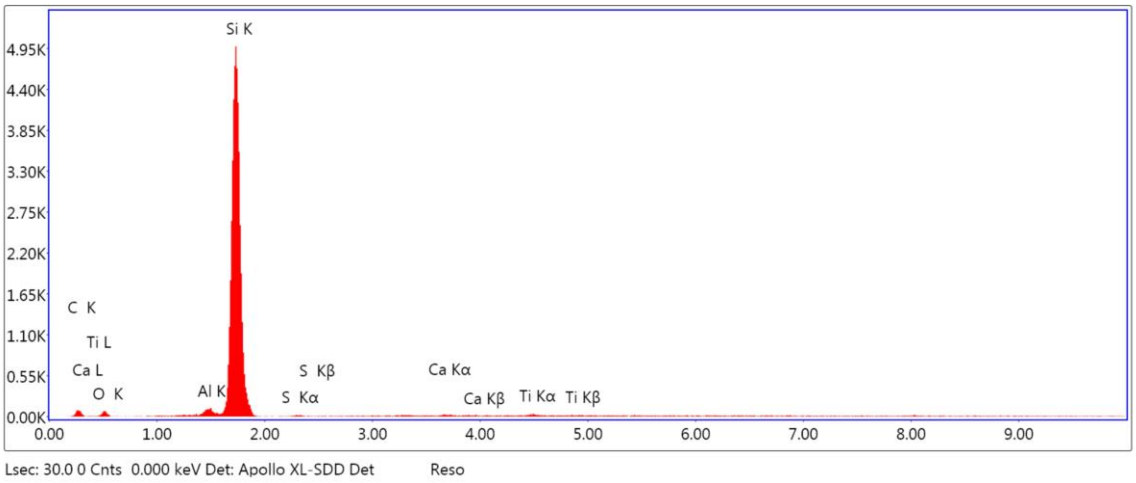

Element	Weight %	Atomic %	Net Int.	Error %
C K	36.01	54.41	16.95	14.65
O K	9.19	10.42	13.5	15.15
AlK	1.14	0.77	28.04	8.78
SiK	52.39	33.86	1452.77	2.49
S K	0.18	0.1	2.32	71.47
CaK	0.44	0.2	7.41	24.49
TiK	0.65	0.25	10.58	18.36

Figure 11b: Area 9 spot 1 element distribution image and quantification from group B specimen

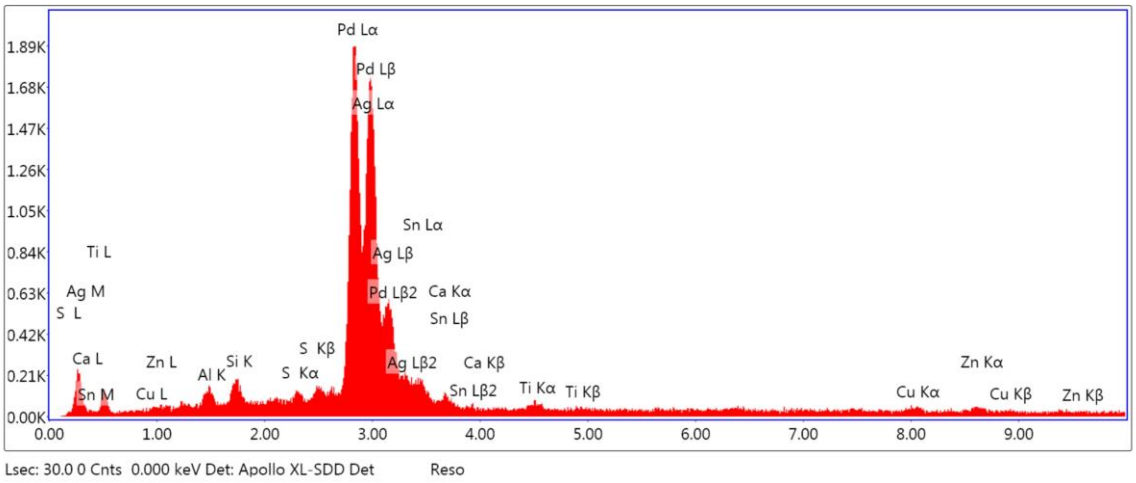

Element	Weight %	Atomic %	Net Int.	Error %
AlK	1.58	5.49	16.23	35.96
SiK	2.08	6.94	30.33	16.76
S K	0.63	1.85	12.98	21.13
PdL	51.56	45.47	613.85	2.52
AgL	31.46	27.36	360.25	4.21
SnL	9.09	7.19	50.48	21.15
CaK	0	0.01	0.05	99.99
TiK	0.94	1.84	11.43	32.92
CuK	1.18	1.74	11.22	30.48
ZnK	1.48	2.12	12.75	27.2

Figure 11c: Area 9 spot 2 element distribution image and quantification from group B specimen

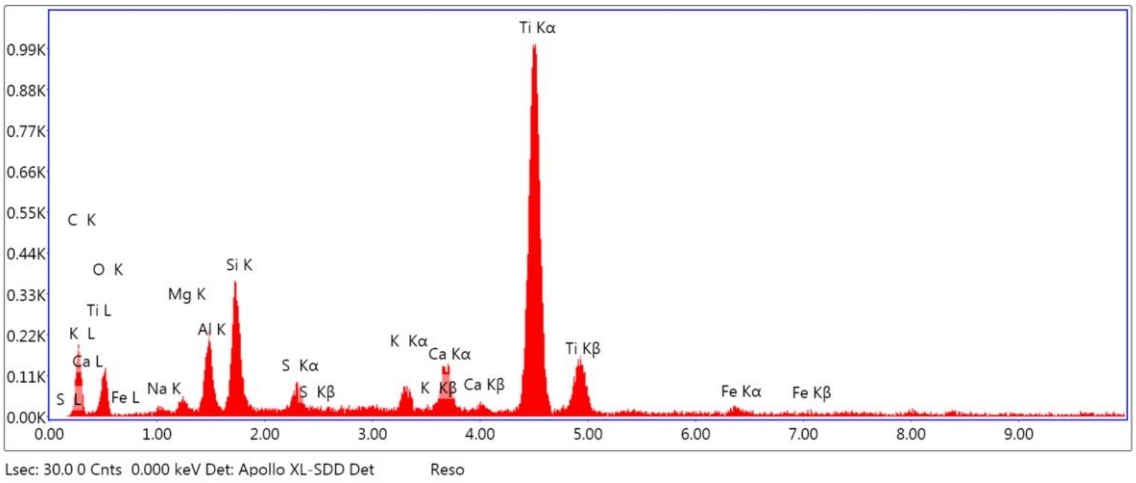

Element	Weight %	Atomic %	Net Int.	Error %
C K	32.9	50.36	36.03	11.2
O K	26.68	30.66	27.66	13.77
NaK	0.58	0.46	2.29	77.2
MgK	0.6	0.46	5.21	41.14
AlK	3.7	2.52	47.59	9.77
SiK	5.7	3.73	94.16	7.79
S K	0.86	0.49	16.56	16.24
K K	0.85	0.4	18.03	14.58
CaK	2.27	1.04	44.39	7.79
TiK	25.22	9.68	409.43	1.84
FeK	0.64	0.21	6.46	33.41

Figure 11d: Area 9 spot 3 element distribution image and quantification from group B specimen

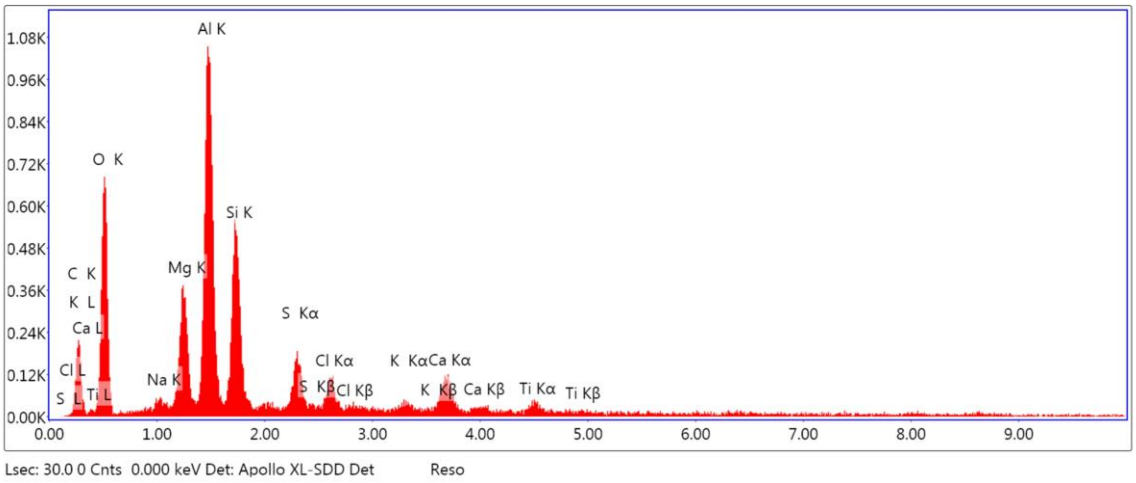

Element	Weight %	Atomic %	Net Int.	Error %
C K	29.56	40.22	42.42	11.69
O K	41.95	42.86	150.67	10.54
NaK	1.37	0.98	13.06	18.62
MgK	5.1	3.43	101.96	8.92
AlK	11.89	7.21	302.28	7.04
SiK	5.79	3.37	155.87	7.59
S K	1.5	0.76	49.02	10.94
ClK	0.86	0.4	29.28	13.18
K K	0.29	0.12	10.35	18.92
CaK	1.24	0.51	40.36	8.56
TiK	0.43	0.15	13.05	17.19

Figure 11e: Area 9 spot 4 element distribution image and quantification from group B specimen

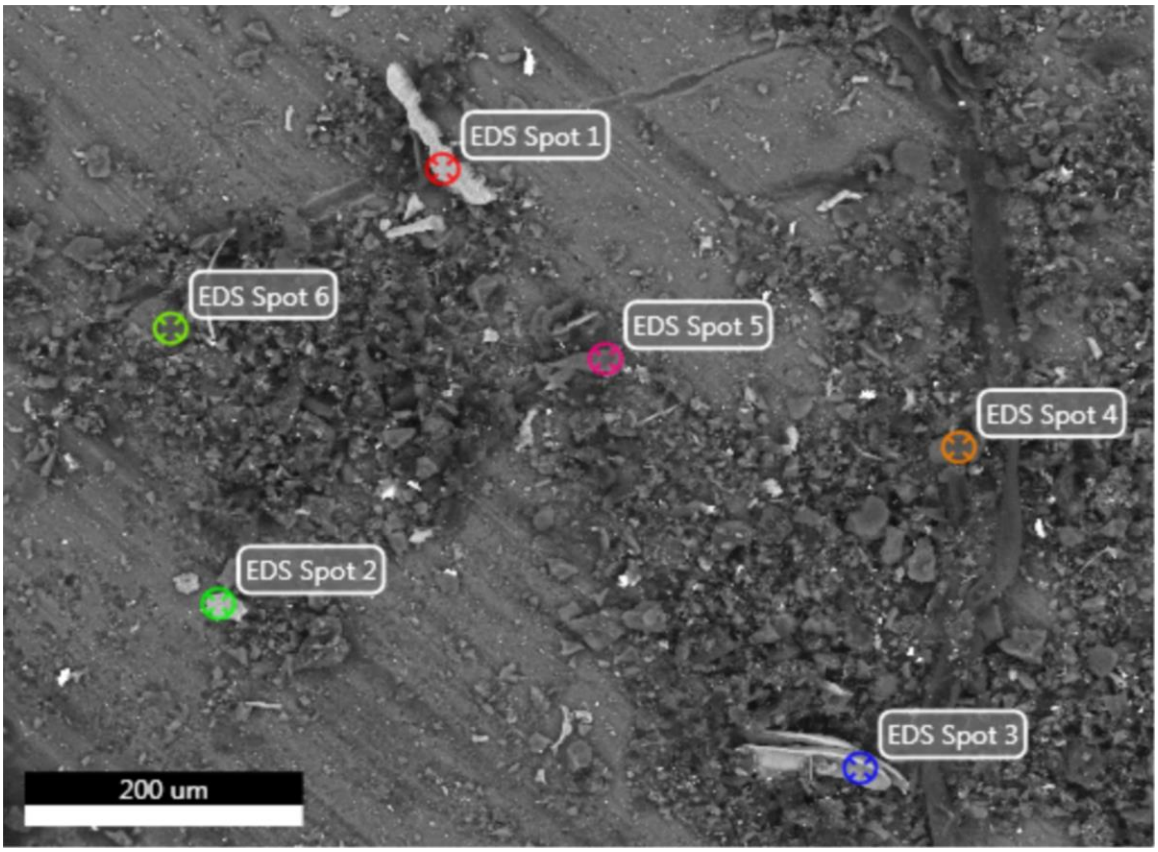

Figure 12a: Micrograph of area 10 showing areas for analysis from group B specimen

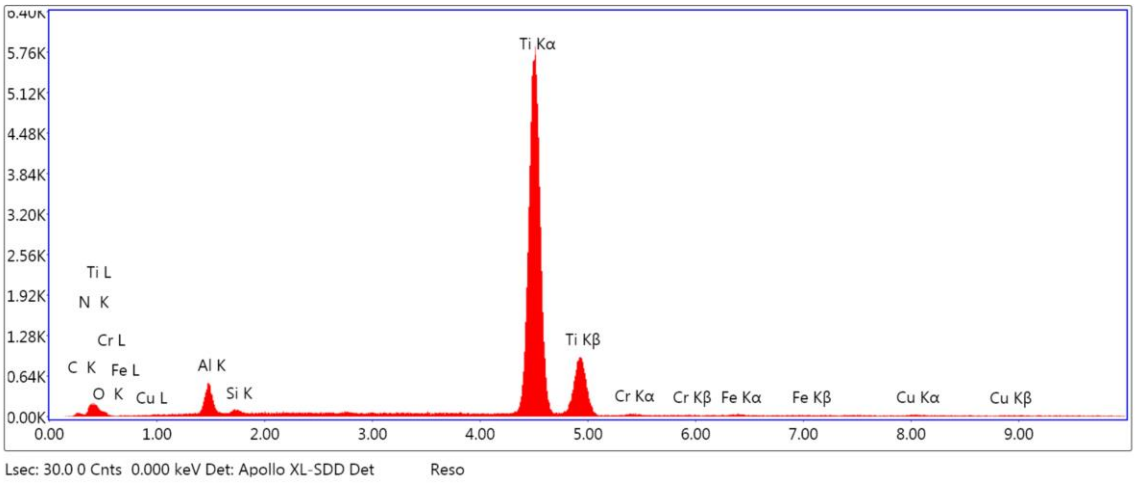

Element	Weight %	Atomic %	Net Int.	Error %
C K	5.83	14.95	13.81	13.31
N K	4.59	10.07	12.6	16.29
O K	11.14	21.43	15.91	15.54
AlK	6.12	6.98	126.18	9.24
SiK	0.56	0.61	14.88	20.79
TiK	70.51	45.29	2387.41	1.11
CrK	0.41	0.24	8.09	44.23
FeK	0.38	0.21	7.08	44.35
CuK	0.46	0.22	6.66	58.61

Figure 12b: Area 10 spot 1 element distribution image and quantification from group B specimen

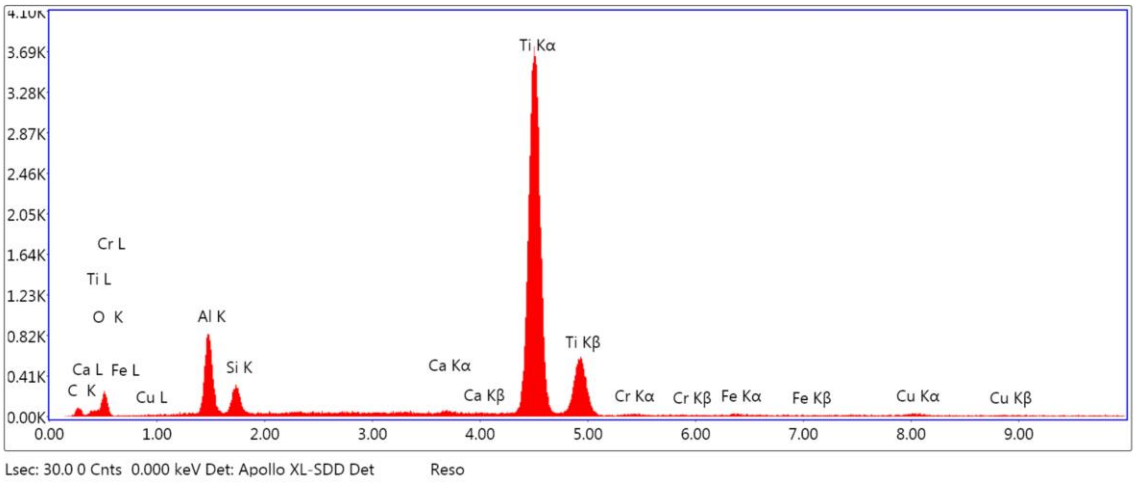

Element	Weight %	Atomic %	Net Int.	Error %
C K	9.65	19.87	18.74	13.5
O K	27.67	42.77	52.35	12.52
AlK	10.03	9.19	222.23	8.36
SiK	3.04	2.68	79.4	10.15
CaK	0.33	0.2	13.56	21.58
TiK	47.77	24.66	1566.62	1.25
CrK	0.22	0.11	4.76	61.24
FeK	0.39	0.17	7.52	33.49
CuK	0.9	0.35	13.09	20.28

Figure 12c: Area 10 spot 2 element distribution image and quantification from group B specimen

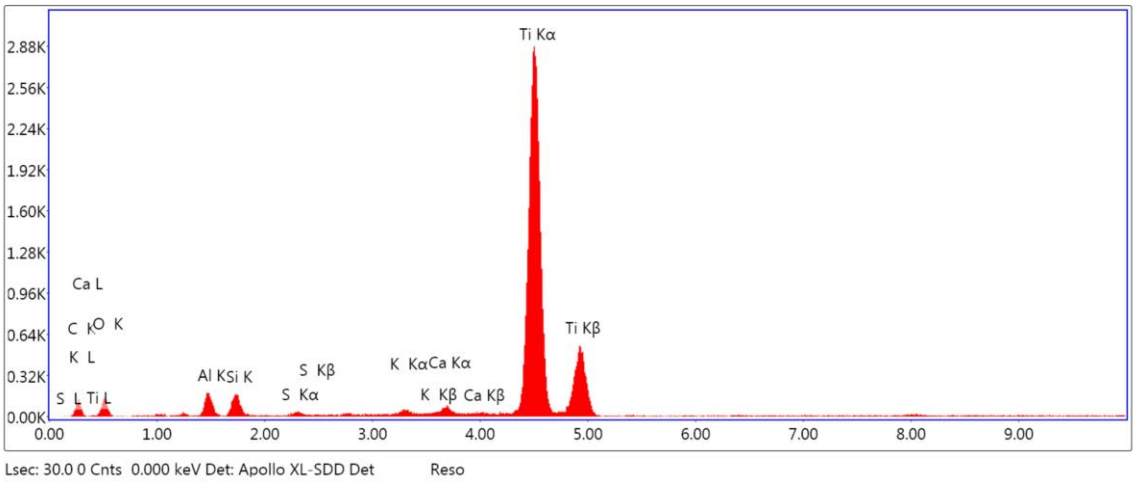

Element	Weight %	Atomic %	Net Int.	Error %
C K	14.12	28.06	24.48	11.68
O K	27.62	41.21	32.02	13.27
AlK	2.5	2.21	36.19	12.47
SiK	1.85	1.57	36.77	11.79
S K	0.01	0.01	0.31	79.16
K K	0.23	0.14	7.22	28.09
CaK	0.58	0.35	17.52	15.09
TiK	53.09	26.46	1192.98	1.38

Figure 12d: Area 10 spot 3 element distribution image and quantification from group B specimen

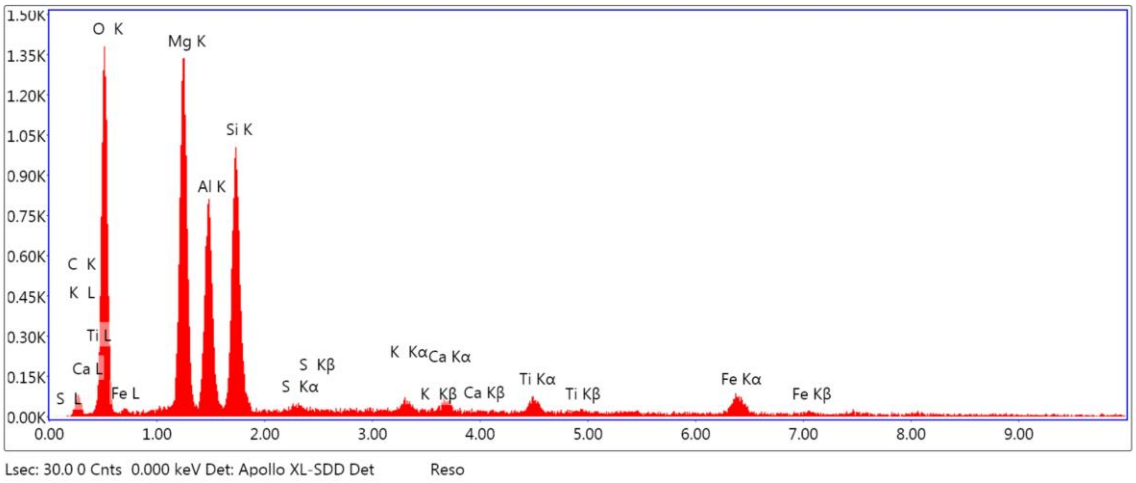

Element	Weight %	Atomic %	Net Int.	Error %
C K	11.04	16.7	14.55	15.09
O K	50.11	56.91	304.94	9.04
MgK	15.88	11.87	349.63	7.83
AlK	9.94	6.69	213.57	8.73
SiK	10.81	6.99	273.61	7.93
S K	0.11	0.06	3.21	70.85
K K	0.22	0.1	8.23	23.47
CaK	0.29	0.13	10.06	22.8
TiK	0.42	0.16	13.84	19.92
FeK	1.17	0.38	25.94	14.85

Figure 12e: Area 10 spot 4 element distribution image and quantification from group B specimen

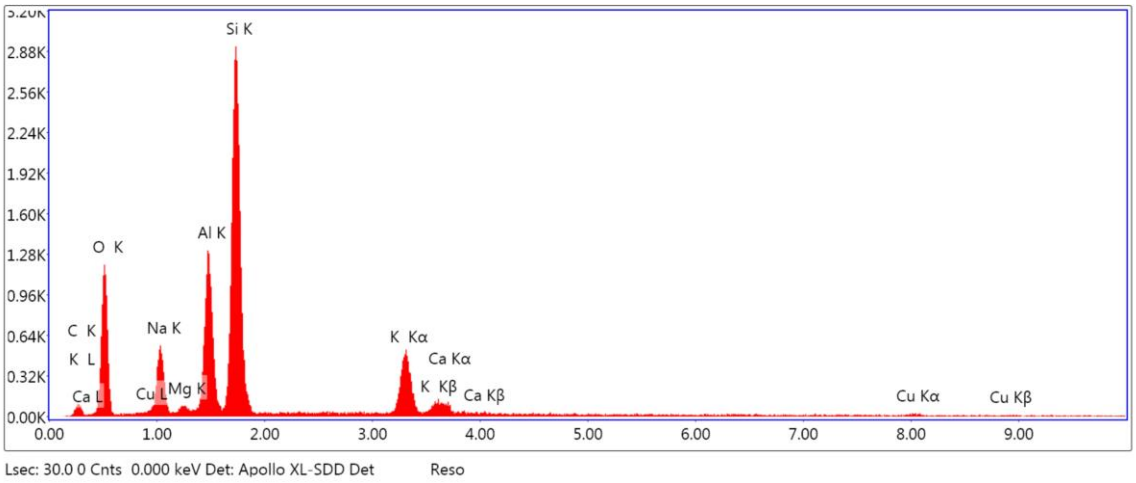

Element	Weight %	Atomic %	Net Int.	Error %
C K	9.13	14.65	13.56	16.1
O K	42.78	51.53	269.91	9.6
NaK	9.72	8.15	137.15	9.89
MgK	0.72	0.57	17.19	16.74
AlK	10.32	7.37	358.08	7.2
SiK	22.31	15.31	846.97	6.42
K K	3.96	1.95	180.06	4.8
CaK	0.82	0.39	33.76	14.78
CuK	0.23	0.07	4.71	59.62

Figure 12f: Area 10 spot 5 element distribution image and quantification from group B specimen

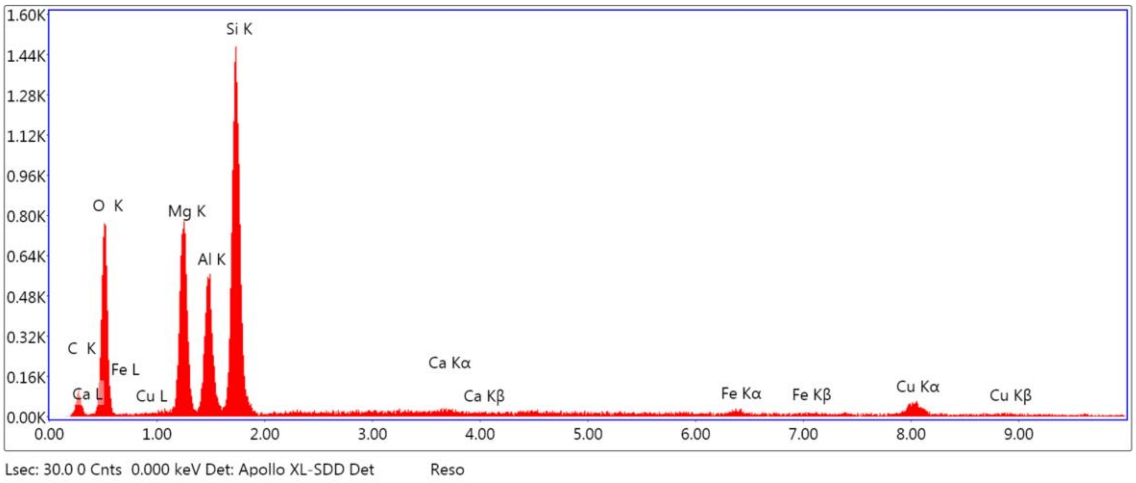

Element	Weight %	Atomic %	Net Int.	Error %
C K	16.6	25.02	16.11	14.75
O K	42.53	48.14	170.25	9.83
MgK	11.92	8.88	210.24	8.04
AlK	8.2	5.5	154.52	8.25
SiK	18.06	11.65	402.54	6.94
CaK	0.18	0.08	4.82	62.78
FeK	0.39	0.13	6.99	59.11
CuK	2.12	0.6	26.62	14.52

Figure 12g: Area 10 spot 6 element distribution image and quantification from group B specimen

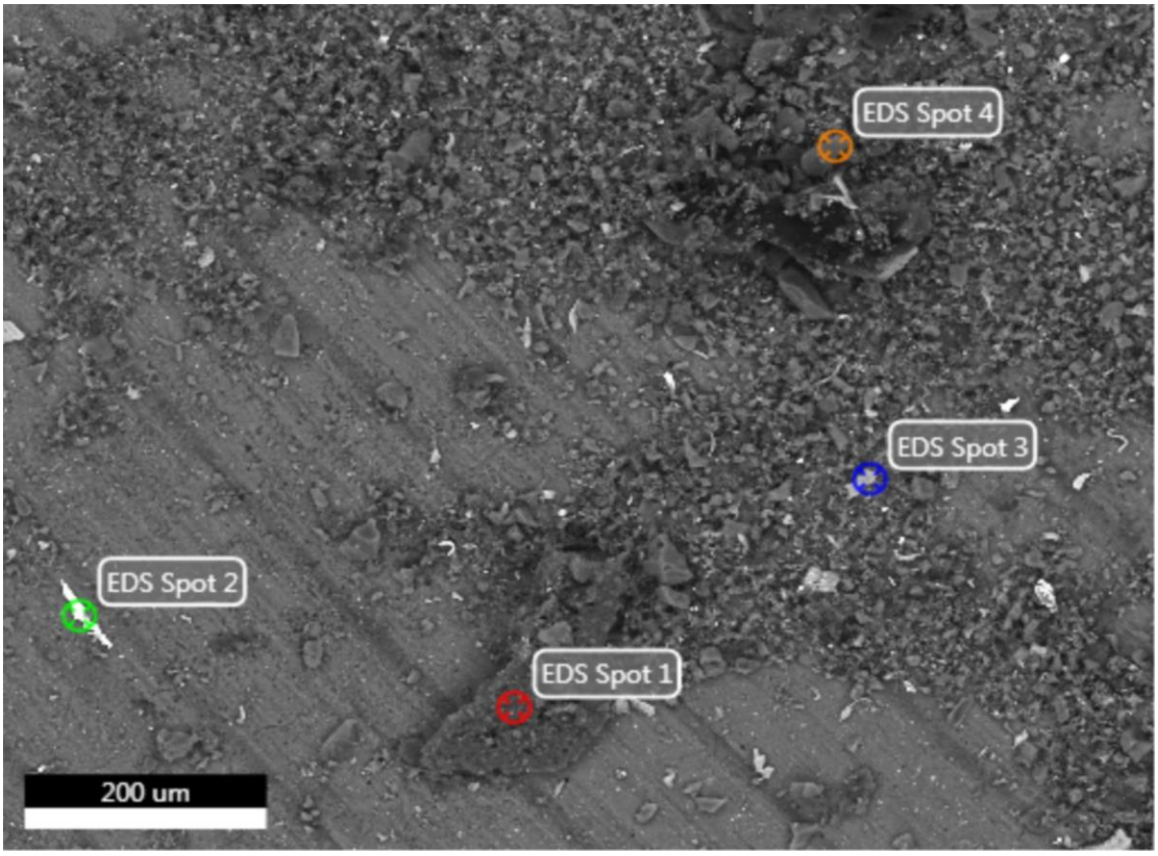

Figure 13a: Micrograph of area 11 showing areas for analysis from group B specimen

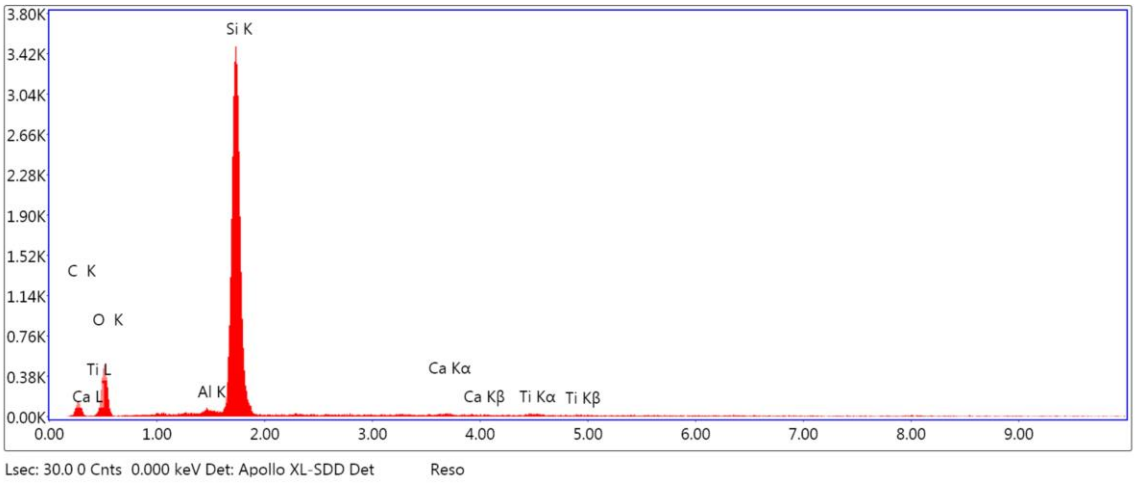

Element	Weight %	Atomic %	Net Int.	Error %
C K	30.38	41.92	29.17	12.64
O K	38.24	39.61	107.52	10.9
AlK	0.45	0.28	11.81	13.43
SiK	30.65	18.09	1026.57	3.83
CaK	0.13	0.05	3.3	61.66
TiK	0.15	0.05	3.65	60.55

Figure 13b: Area 11 spot 1 element distribution image and quantification from group B specimen

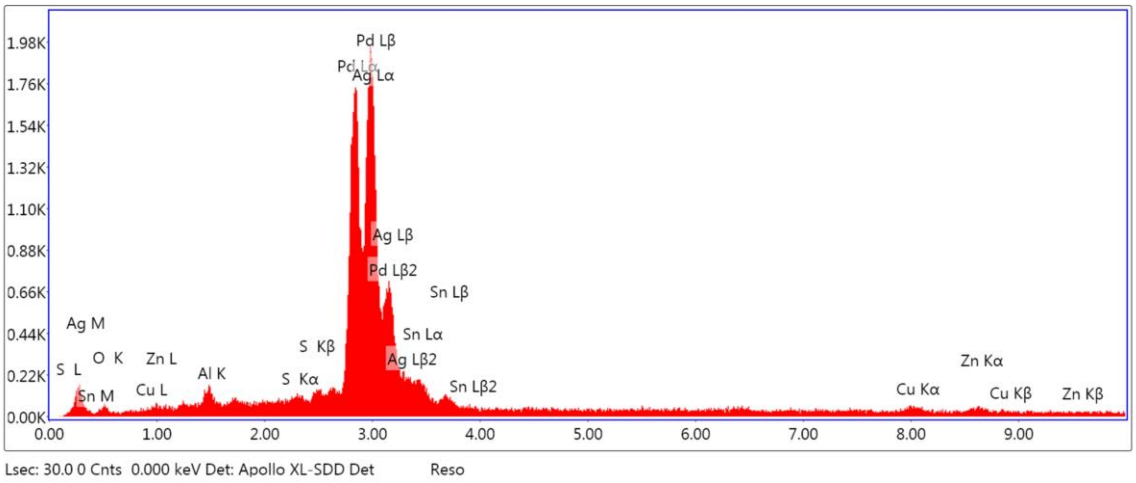

Element	Weight %	Atomic %	Net Int.	Error %
O K	6.17	28.77	8.99	26.71
AlK	1.91	5.29	21.29	17.87
S K	0.71	1.64	16.14	15.46
PdL	43.63	30.59	572.51	2.33
AgL	36.09	24.96	457.12	3.19
SnL	8.62	5.42	53.67	18.46
CuK	1.5	1.76	15.52	24.57
ZnK	1.37	1.57	12.9	28.87

Figure 13c: Area 11 spot 2 element distribution image and quantification from group B specimen

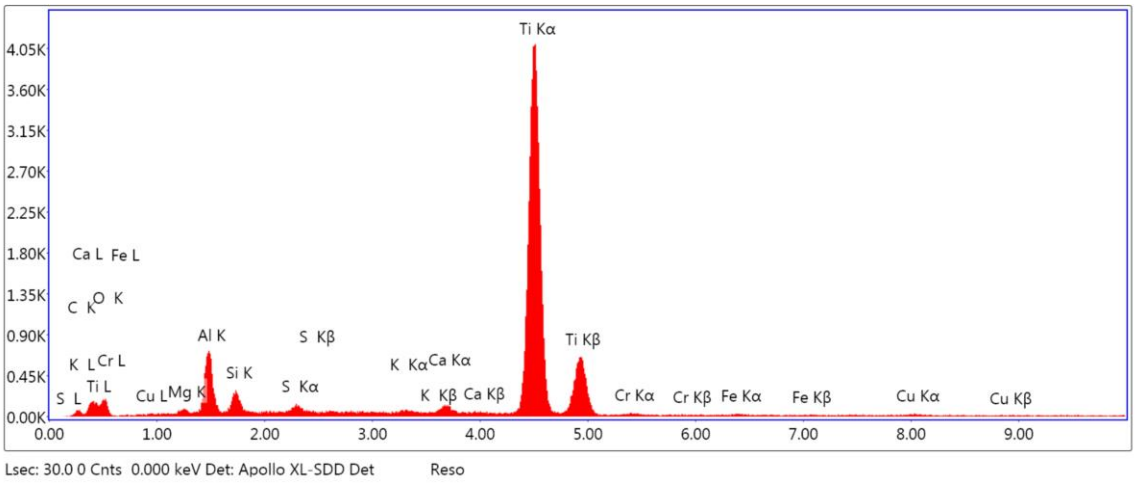

Element	Weight %	Atomic %	Net Int.	Error %
C K	6.53	14.55	12.02	16.87
O K	24.76	41.43	41.8	13.42
MgK	0.73	0.8	9.95	35.52
AlK	9.24	9.17	190.35	8.76
SiK	2.56	2.44	63.61	10.98
S K	0.65	0.54	22.13	17.95
K K	0.23	0.16	9.39	22
CaK	0.82	0.54	32.57	12.77
TiK	53.76	30.04	1679.58	1.32
CrK	0.21	0.11	4.06	63.13
FeK	0.15	0.07	2.79	63.65
CuK	0.36	0.15	5.01	59.39

Figure 13d: Area 11 spot 3 element distribution image and quantification from group B specimen

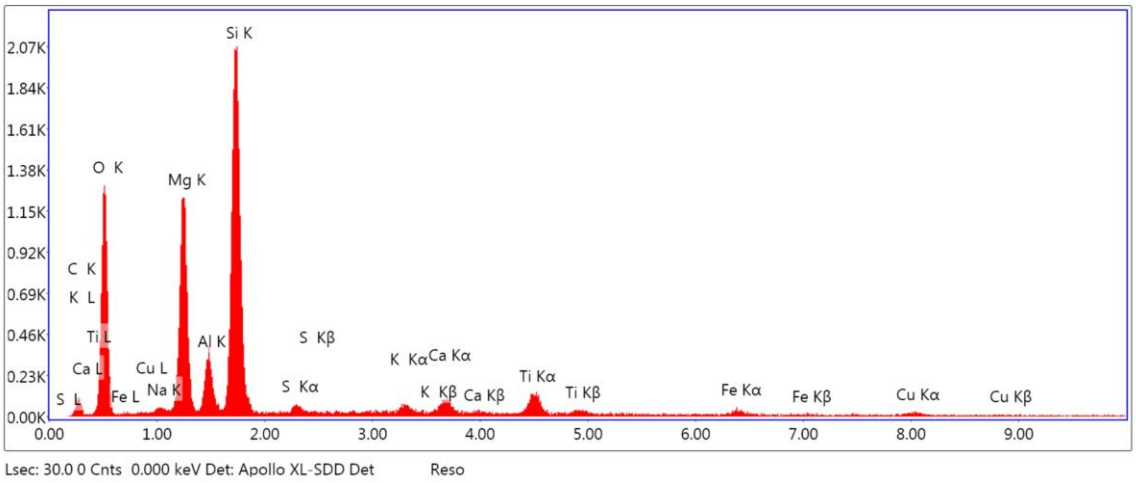

Element	Weight %	Atomic %	Net Int.	Error %
C K	12.66	19.24	18.63	14.94
O K	47.63	54.35	286.62	9.45
NaK	0.7	0.55	8.06	25.32
MgK	13.52	10.15	333.48	7.94
AlK	3.5	2.37	90.17	9.57
SiK	18.05	11.73	614.13	6.54
S K	0.38	0.22	13.17	19.94
K K	0.47	0.22	19.89	15.13
CaK	0.8	0.37	31.52	13.35
TiK	1.31	0.5	48.41	7.57
FeK	0.49	0.16	12.55	20.32
CuK	0.49	0.14	8.9	25.06

Figure 13e: Area 11 spot 4 element distribution image and quantification from group B specimen

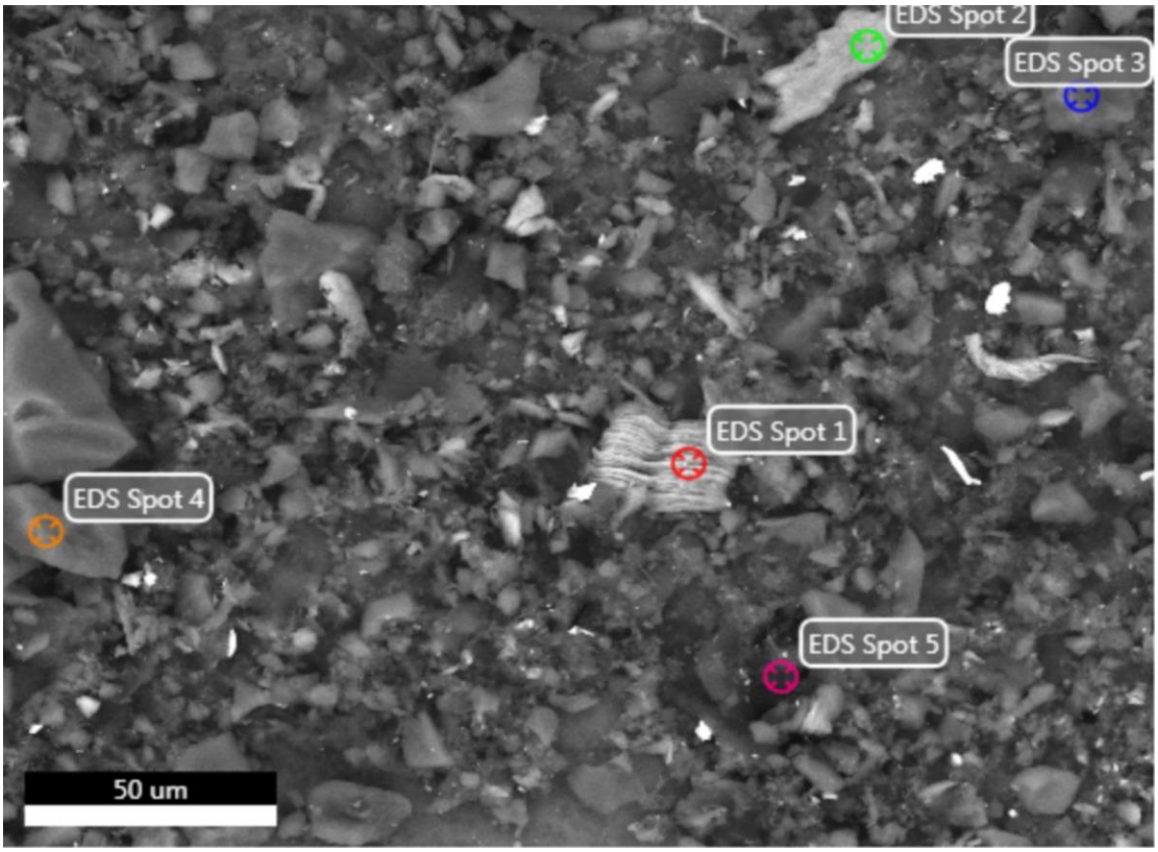

Figure 14a: Micrograph of area 12 showing areas for analysis from group B specimen

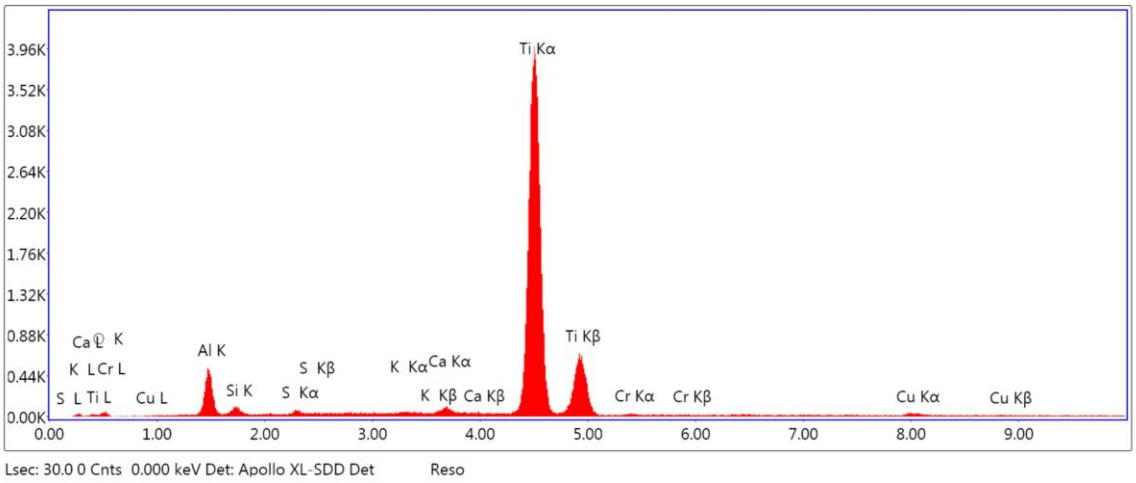

Element	Weight %	Atomic %	Net Int.	Error %
O K	10.89	25.12	10.38	17.75
AlK	9.41	12.87	124.19	9.46
SiK	1.15	1.51	18.64	21.9
S K	0.26	0.3	6.14	63.65
K K	0.34	0.32	9.97	28.04
CaK	1.01	0.93	29.59	13.94
TiK	74.8	57.63	1633.26	1.42
CrK	0.58	0.41	7.35	63.03
CuK	1.55	0.9	14.7	20.63

Figure 14b: Area 12 spot 1 element distribution image and quantification from group B specimen

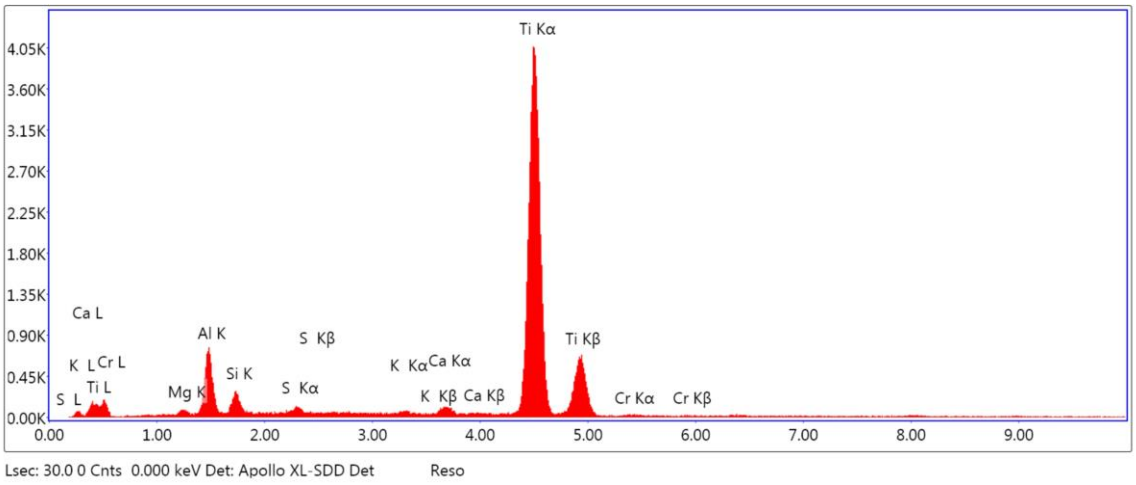

Element	Weight %	Atomic %	Net Int.	Error %
MgK	1.3	2.21	12.52	22.22
AlK	13.87	21.24	198.04	8.85
SiK	4.34	6.38	69.51	10.77
S K	1.21	1.55	26.67	15.49
K K	0.46	0.48	13.13	22.6
CaK	1.21	1.25	34.38	13.98
TiK	76.97	66.38	1679.74	1.63
CrK	0.64	0.51	8.04	33.79

Figure 14c: Area 12 spot 2 element distribution image and quantification from group B specimen

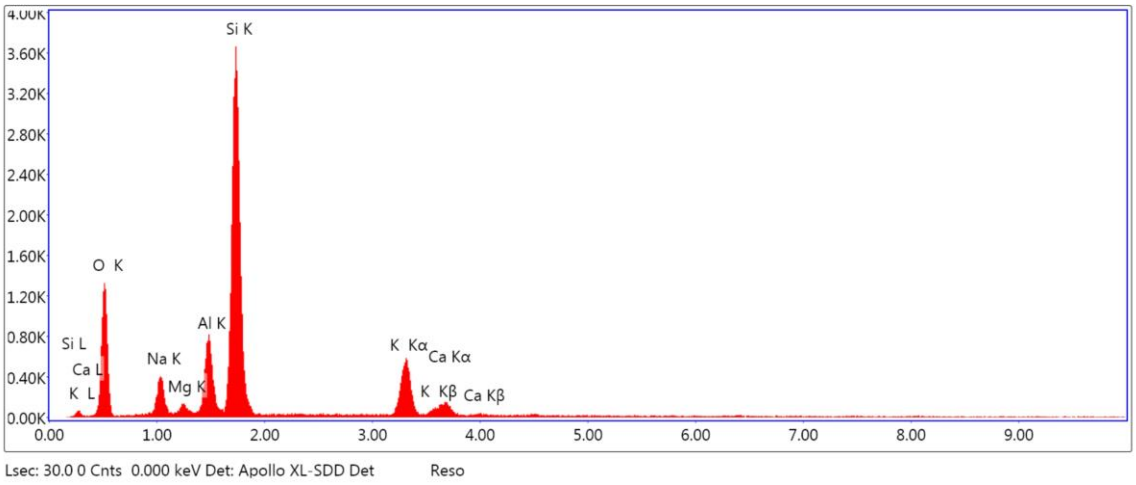

Element	Weight %	Atomic %	Net Int.	Error %
O K	47.3	60.88	296.72	9.4
NaK	8.67	7.77	105.07	10.17
MgK	1.38	1.17	29.27	14.26
AlK	7.17	5.48	218.26	7.84
SiK	29.22	21.43	1039.59	6.09
K K	5.01	2.64	196.19	4.86
CaK	1.24	0.64	43.96	11.66

Figure 14d: Area 12 spot 3 element distribution image and quantification from group B specimen

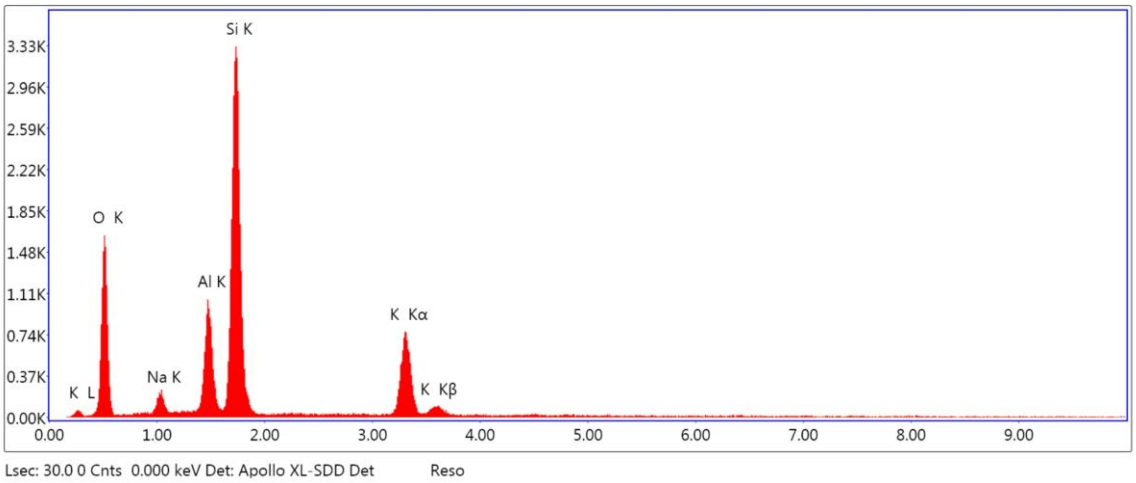

Element	Weight %	Atomic %	Net Int.	Error %
O K	52.97	66.53	357.57	9.08
NaK	5.57	4.87	64.21	11.1
AlK	8.66	6.45	284.84	7.15
SiK	26.29	18.81	969.27	6.04
K K	6.51	3.34	266.97	4.16

Figure 14e: Area 12 spot 4 element distribution image and quantification from group B specimen

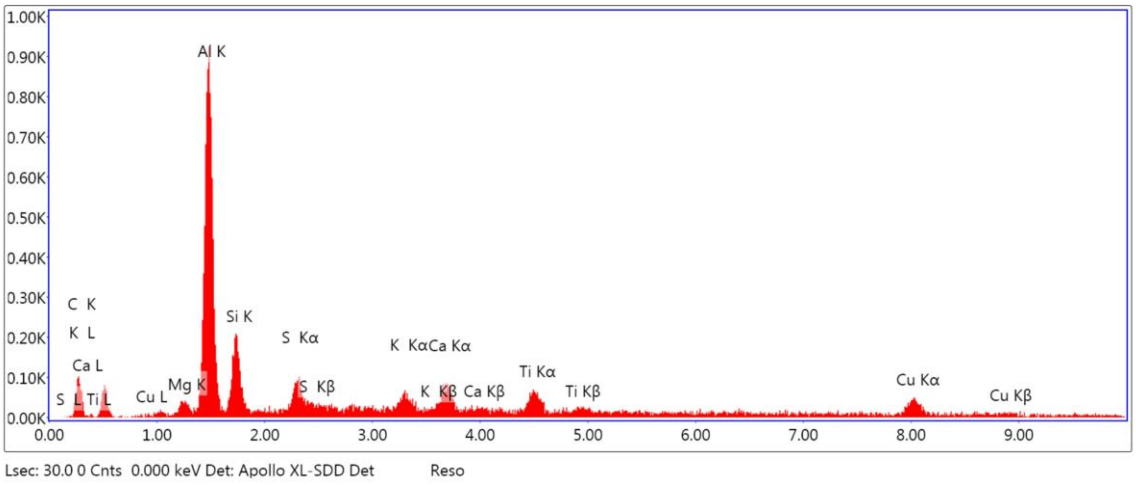

Element	Weight %	Atomic %	Net Int.	Error %
C K	54.94	75.78	19.34	14.33
MgK	0.1	0.07	0.73	74.45
AlK	24.61	15.11	239.71	5.56
SiK	6.9	4.07	48.96	11.23
S K	2.47	1.28	21.28	17.07
K K	1.51	0.64	14.7	18.64
CaK	2.49	1.03	22.12	15.56
TiK	2.49	0.86	20.63	14.67
CuK	4.48	1.17	18.3	15.59

Figure 14f: Area 12 spot 5 element distribution image and quantification from group B specimen

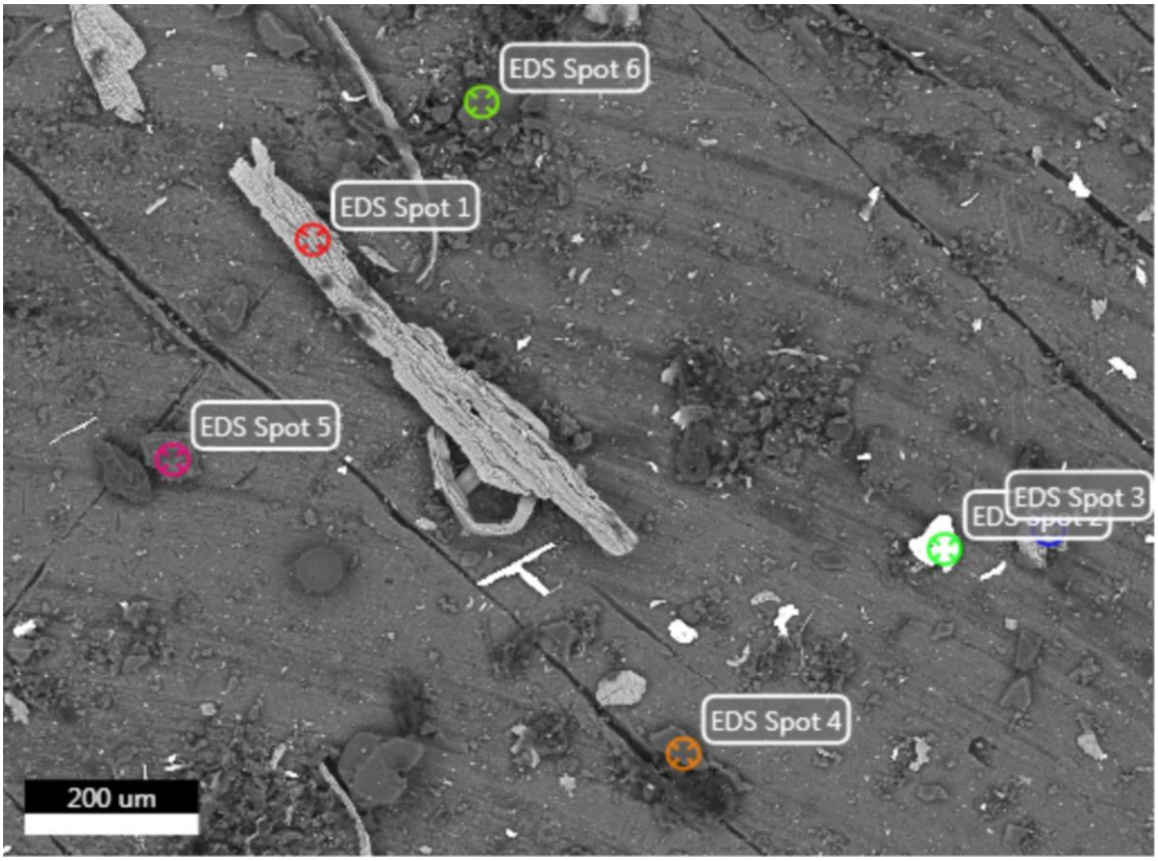

Figure 15a: Micrograph of area 13 showing areas for analysis from group B specimen

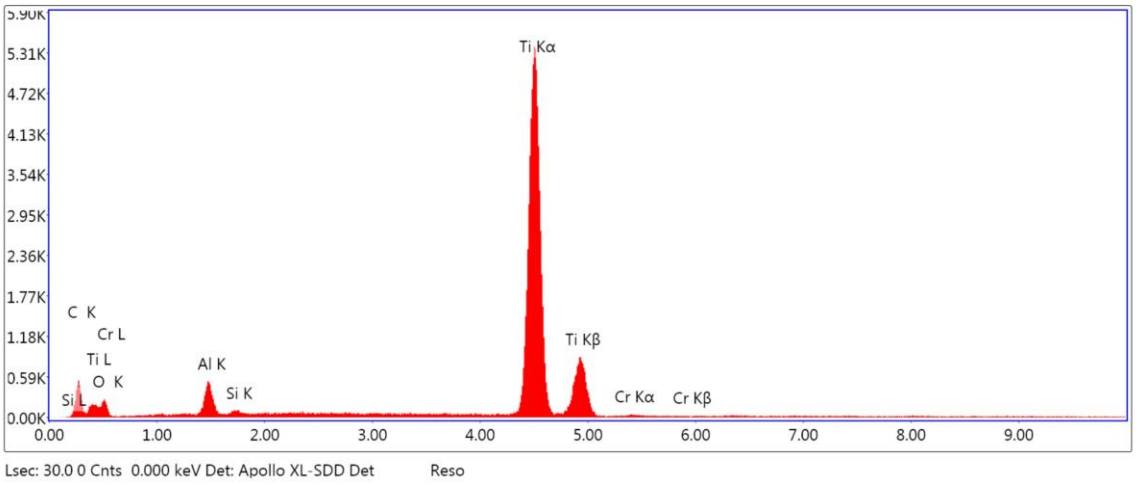

Element	Weight %	Atomic %	Net Int.	Error %
C K	27.57	48.12	110.34	8.62
O K	21.58	28.28	51.73	12.66
AlK	3.8	2.95	124.43	9.02
SiK	0.23	0.17	9.9	27.18
TiK	46.5	20.35	2218.48	1.37
CrK	0.31	0.12	9.43	27.48

Figure 15b: Area 13 spot 1 element distribution image and quantification from group B specimen

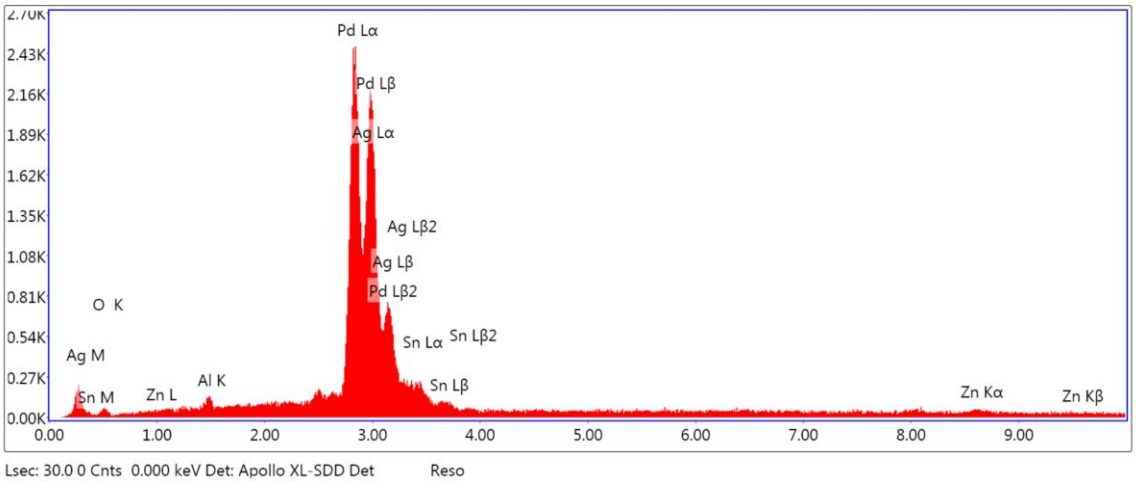

Element	Weight %	Atomic %	Net Int.	Error %
O K	5.47	27.41	8.96	20.96
AlK	0.7	2.08	8.9	53.05
PdL	53.67	40.48	815.94	1.96
AgL	29.83	22.19	433.83	3.54
SnL	8.79	5.95	60.89	18
ZnK	1.54	1.89	16.55	25.03

Figure 15c: Area 13 spot 2 element distribution image and quantification from group B specimen

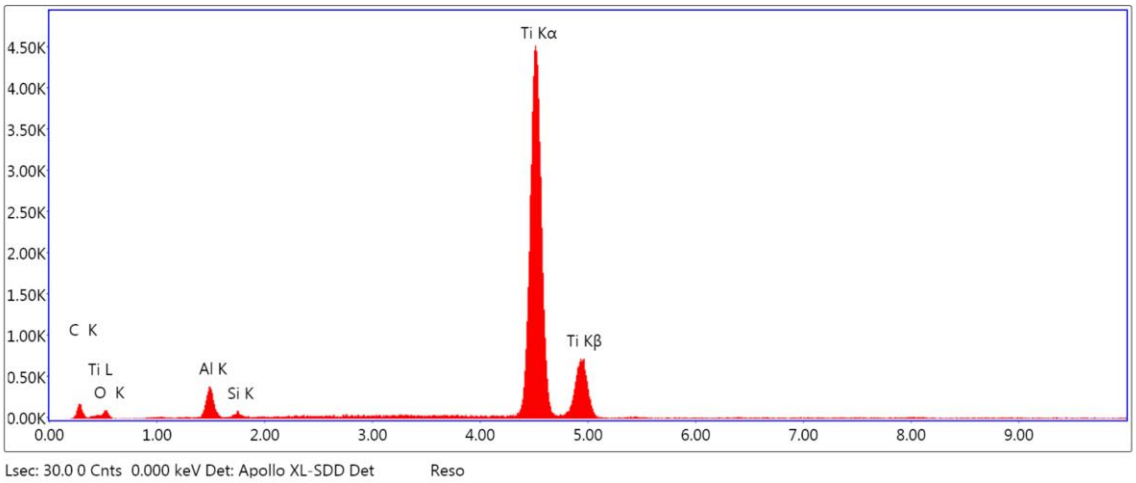

Element	Weight %	Atomic %	Net Int.	Error %
C K	16.49	35.45	38.41	10.26
O K	16.36	26.39	22.08	14.53
AlK	4.55	4.35	87.16	10.09
SiK	0.19	0.17	4.73	66.26
TiK	62.41	33.64	1878.07	1.29

Figure 15d: Area 13 spot 3 element distribution image and quantification from group B specimen

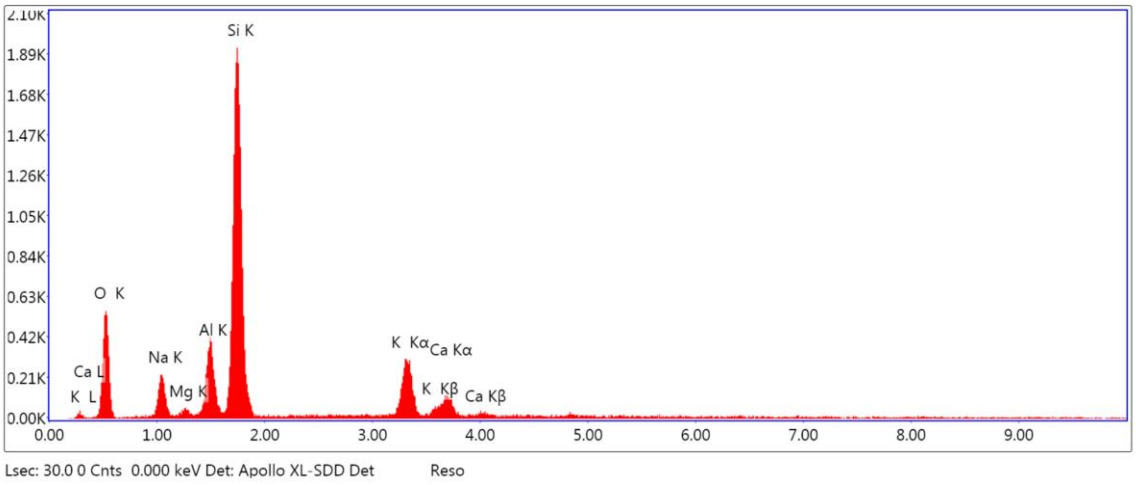

Element	Weight %	Atomic %	Net Int.	Error %
O K	44.63	58.58	126.43	10.19
NaK	8.65	7.9	52.65	11.62
MgK	0.69	0.6	7.33	31.15
AlK	6.87	5.35	106.41	8.27
SiK	31.21	23.33	564.24	6.16
K K	5.69	3.05	109.86	5.79

Figure 15e: Area 13 spot 4 element distribution image and quantification from group B specimen

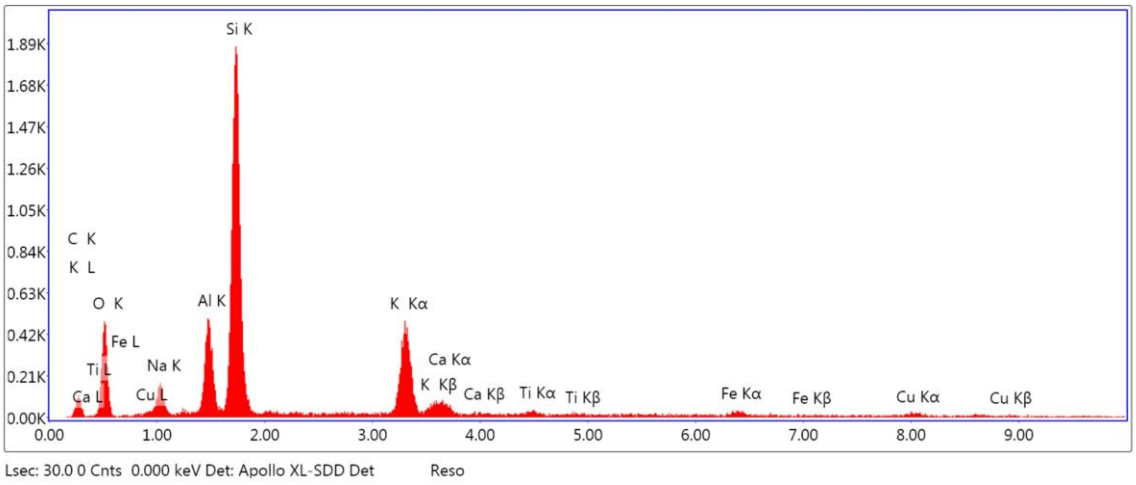

Element	Weight %	Atomic %	Net Int.	Error %
C K	19.58	29.69	18.19	14.28
O K	38.95	44.35	104.01	10.88
NaK	4.94	3.91	35.51	12.23
AlK	6.04	4.08	123.62	7.82
SiK	21.88	14.19	526.29	5.85
K K	6.28	2.92	161.91	4.54
CaK	0.75	0.34	16.99	17.9
TiK	0.26	0.1	5.7	41.7
FeK	0.6	0.2	9.23	24
CuK	0.73	0.21	7.99	26.84

Figure 15f: Area 13 spot 5 element distribution image and quantification from group B specimen

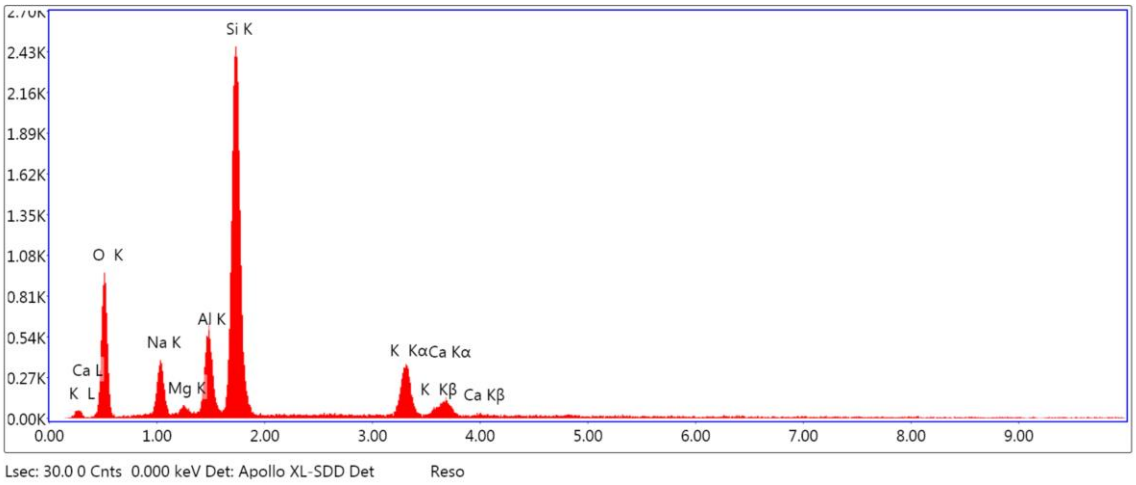

Element	Weight %	Atomic %	Net Int.	Error %
O K	46.11	59.52	211.35	9.57
NaK	10.51	9.45	94.16	10.23
MgK	1.18	1	17.58	13.57
AlK	7.3	5.59	157.4	8.14
SiK	29.09	21.39	734.94	6.28
K K	4.32	2.28	122.15	5.69
CaK	1.49	0.77	38.12	13.92

Figure 15g: Area 13 spot 6 element distribution image and quantification from group B specimen

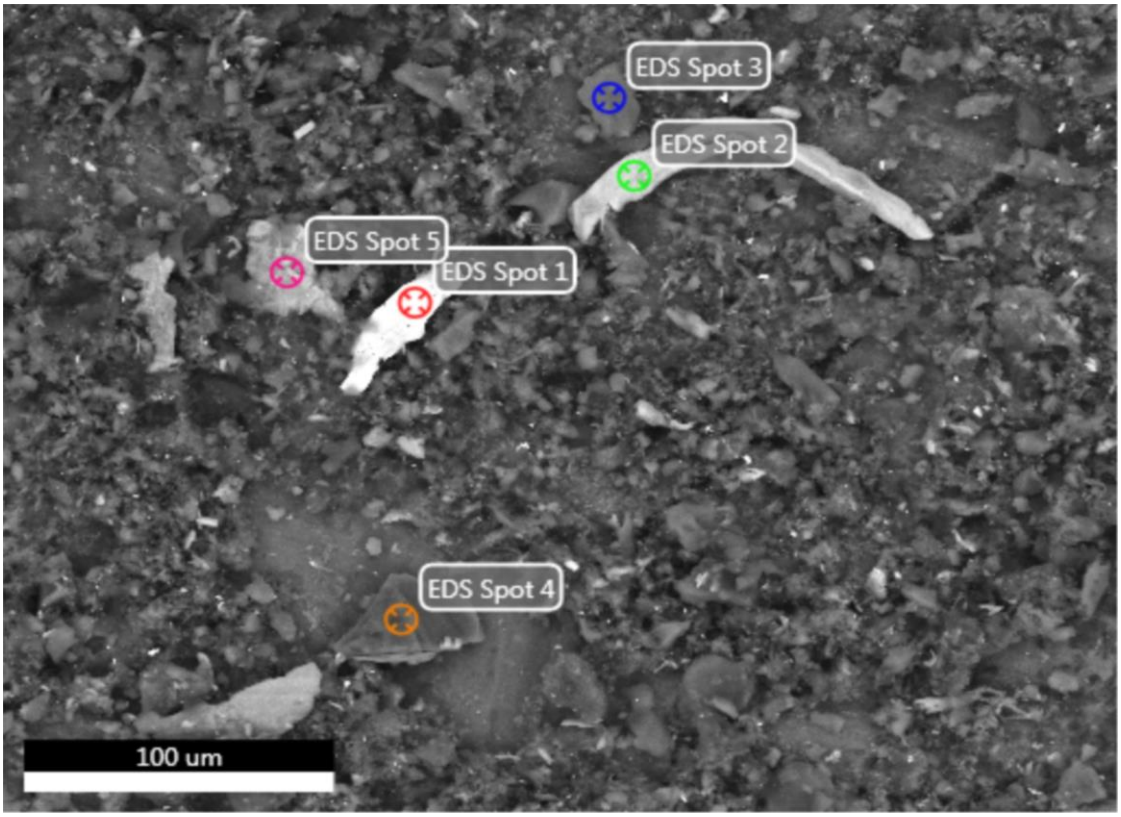

Figure 16a: Micrograph of area 14 showing areas for analysis from group B specimen

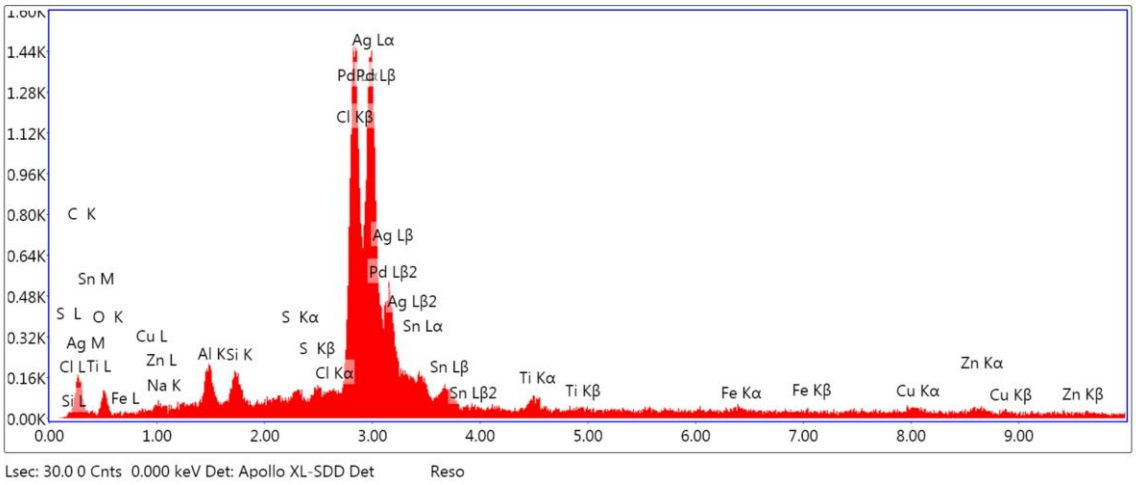

Element	Weight %	Atomic %	Net Int.	Error %
C K	7.98	28.16	19.24	11.92
O K	12.02	31.84	18.38	15.81
NaK	0.01	0.02	0.03	99.99
AlK	3.19	5.02	38.13	13.98
SiK	2.13	3.22	34.91	13.45
S K	0.85	1.13	19.26	18.57
ClK	0.07	0.09	1.74	71.37
PdL	37.43	14.91	483.89	2.25
AgL	24.28	9.54	304.57	3.9
SnL	7.33	2.62	49.8	16.96
TiK	1.35	1.19	19.49	21.77
FeK	0.68	0.51	8.74	41.06
CuK	1.3	0.87	13.19	26.23
ZnK	1.39	0.9	12.73	27.02

Figure 16b: Area 14 spot 1 element distribution image and quantification from group B specimen

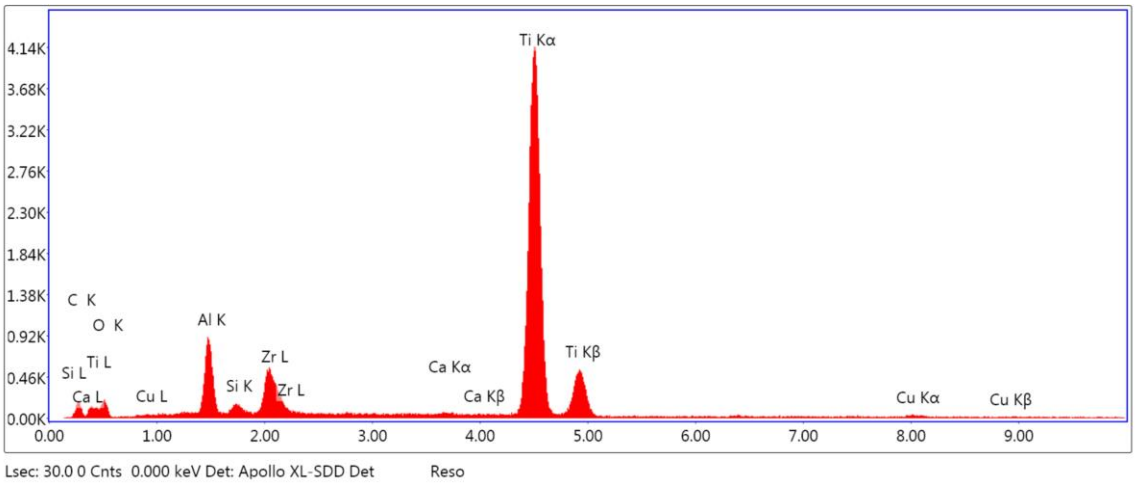

Element	Weight %	Atomic %	Net Int.	Error %
C K	17.37	35.26	39.72	11.21
O K	20.46	31.18	43.63	12.84
AlK	8.56	7.74	238.57	8.32
SiK	0.88	0.77	29.45	14.43
ZrL	7.1	1.9	145.22	5.85
CaK	0.24	0.14	11.09	32.45
TiK	44.64	22.73	1730.86	1.47
CuK	0.76	0.29	13.45	22.91

Figure 16c: Area 14 spot 2 element distribution image and quantification from group B specimen

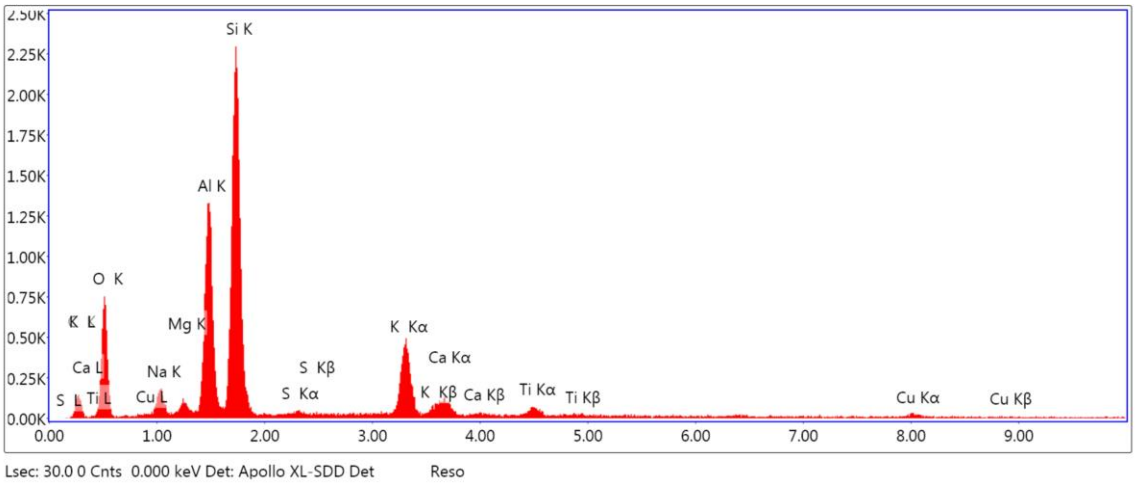

Element	Weight %	Atomic %	Net Int.	Error %
C K	20.12	30.27	27.34	13.13
O K	38.62	43.62	159.78	10.51
NaK	3.39	2.66	38.59	12.75
MgK	0.79	0.58	17.74	16.19
AlK	11.23	7.52	363.35	6.61
SiK	19.5	12.55	655.16	6.17
S K	0.16	0.09	5.16	31.31
K K	4.13	1.91	160.86	4.61
CaK	0.95	0.43	33.19	13.65
TiK	0.6	0.23	19.93	15.78
CuK	0.51	0.15	8.58	26.8

Figure 16d: Area 14 spot 3 element distribution image and quantification from group B specimen

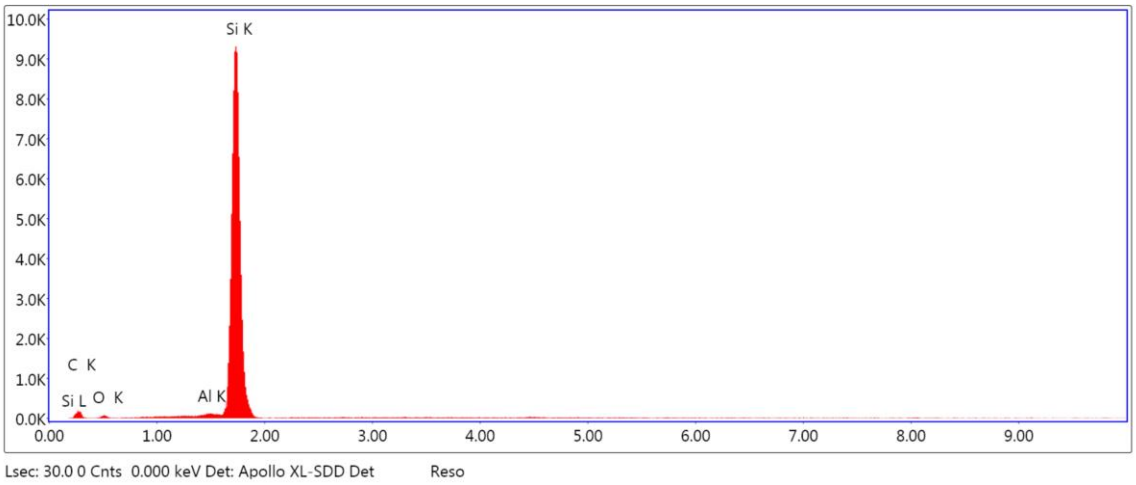

Element	Weight %	Atomic %	Net Int.	Error %
C K	43.84	63	41.3	12.49
O K	5.31	5.73	13.94	16.35
AlK	0.46	0.29	22.1	11.09
SiK	50.39	30.97	2775.28	1.97

Figure 16e: Area 14 spot 4 element distribution image and quantification from group B specimen

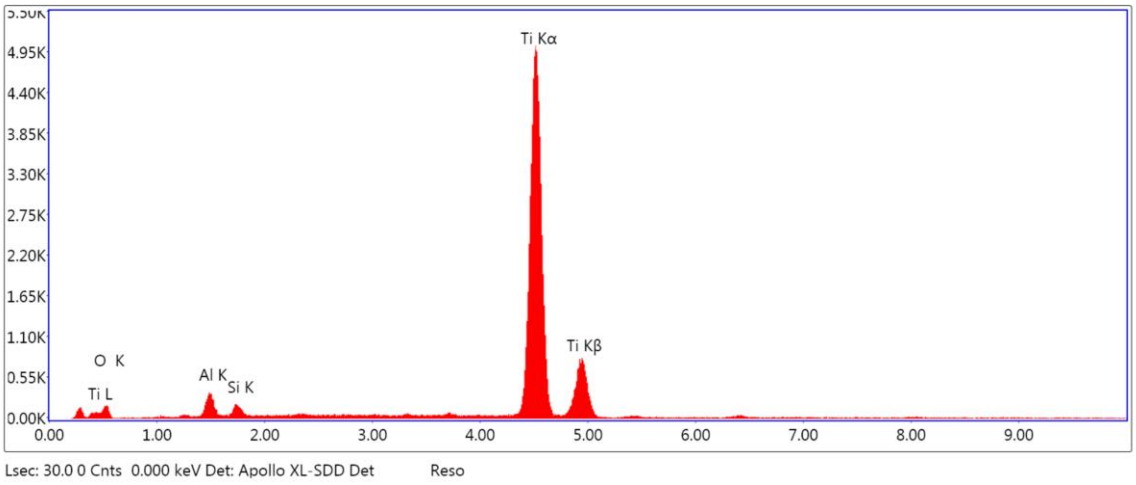

Element	Weight %	Atomic %	Net Int.	Error %
O K	26.17	49.87	39.31	13.08
AlK	4.76	5.38	88.44	10.27
SiK	1.79	1.94	44.49	11.95
TiK	67.28	42.81	2086.59	1.14

Figure 16f: Area 14 spot 5 element distribution image and quantification from group B specimen

DISCUSSION

The present study focused on identification and evaluation of particles that were collected from dental implant abutment screws. All the samples that were used for debris collection had passed all the laboratory steps of fabrication of custom abutment and definitive prosthesis. Therefore, debris could have been influenced by different steps of milling, fabrication and preparation in the laboratory. The ultrasonic cleaning of screws immersed in ethyl alcohol was the method used which had been shown to have better results for separating particles in previous studies[9] and therefore was selected for the present study to collect debris.

Identification of Debris and Possible Source of Contamination

Examination of scanning electron microscopy and energy-dispersive spectroscopy images identified multiple elements in contaminant debris. These elements can be classified into two groups: elements that can be found in the material that were used for fabrication of abutment or definitive prostheses and elements that can't be found in the restorative materials and instruments that were used for fabrication of abutments or definitive prostheses. A major part of elements were categorized in the first group, for example Ti, Al and V are the elements of titanium alloy (Ti 6Al-4V) used for the fabrication of custom abutment. Traces of Zr and Y elements can be related to zirconia custom abutment or the YSZ (yttria-stabilized zirconia) restorative crown. The feldspar ($KAlSi_3O_8$– $NaAlSi_3O_8$– $CaAl_2Si_2O_8$), kaolinite ($Al_2Si_2O_5(OH)_4$)and quartz (SiO2) in porcelain used for layering Zr core or PFM restoration and lithium disilicate in IPS EMax

crowns can be the source of trace elements Si, Na, K, Al, Ca, La and O. Metallic alloys used for fabrication of PFM restoration can contain elements such as Cu, Pd, Ag, Zn, Sn and many instruments are made of steel, which could be a source of Fe, Ni and Cr. Since no metal alloy was used in group A, the particles containing metallic elements could have been transferred from other sources during the laboratory procedures. Also some metallic elements like Cr, Nb and Fe found in group B can't be related to PFM metal alloy used for fabrication of crown since they should be found only in base metal alloys. The body of dental burs can be another source of contamination with iron, nickel and chromium. High atomic percentage of aluminum in some spots can be related to aluminum stubs used for specimen mounting and not necessarily the particles. The coating procedure needed for detection of gold in specimens was not done and it can explain why no trace of gold element was found in specimens.

Contaminant particles containing carbon can be related to lubricant that is used during milling process of custom abutments or finishing devices like rubber wheels in both groups A and B. Finding traces of calcium and sulfur can also be related to procedures with dental stones.

These finding confirms that debris can be transferred to abutment screw not only from the same abutment or prosthesis but also other sources in dental laboratories during fabrication and finishing

Possible Effects of Abutment Screw Contamination

Presence of particles on abutment screws may negatively affect preload in the implant abutment joint. After applying a tightening torque to abutment screw, the friction between screw thread and the mating threads of the implant contributes to the process.

The elongation of the screw causes tension in the screw and elastic recovery of the screw pulls the parts together, creating a compressive clamping force. Any irregularity on the mating surface of the screw and implant may reduce the final preload in the abutment screw by third body interaction at the screw interface. In the present study, the results showed that the particles with different sizes, shapes and chemistries were found on the implant screw surfaces. These particles could originate from the same abutment/prosthesis or from transfer from other sources in dental laboratories during the fabrication process. Placement of the definitive prostheses using these contaminated screws could be one of the possible causes of the screw loosening because of failure of achieving preloads due to presence of particles between mating surface of abutment screw and implant. This would need to be confirmed by future studies.

After evaluation of these results, other concerns may exist because of chemistries of particles entrapped on the screw surface. For example, previous studies have shown galvanic corrosion behavior of dental alloys when coupled with titanium[12 13 14]. We found base metals like Cr, Ni, Cu and Fe in the particles and these elements may initiate active galvanic corrosion with titanium after infiltration of saliva into implant abutment joint. The galvanic corrosion may also be started between different types of metallic particles that are present in the entrapped contaminants.

Previous studies have shown that released metal ions, particularly Cu, Ni, Be, and abraded micro-particles may also induce inflammation of the adjacent periodontal tissues and oral mucosa. Investigators have reported that Cu, Ni, and Be and other elements have pronounced cytotoxic potency. There is also evidence from in vitro investigations that various metallic elements, like Ni, Co, and Cr can influence immune responses in some

situations[15].

CONCLUSION

Debris collected from implant abutment screws showed very different morphological characteristics. The size of particles varied from submicron up to 300 micrometers in ZrO2 abutments and 600 micrometers in titanium abutments. Most of particles were found to be smaller than 50 microns.

The shapes of particles were of many different shapes but they appeared to be predominantly irregular in shape. The elemental analysis of particles by SEM-EDX showed a variety of elements that may have originated directly inside the restorative materials that were used for definitive prosthesis or transferred from other sources during the dental laboratory fabrication process.

The hypothesis was that SEM analysis of entrapped debris along implant screw threads and connections would show different particle shapes, sizes and elemental chemistries. The results of this study showed this hypothesis to be valid.

The analysis of debris collected from implant abutment screw led to concerns about biomechanical and biological interactions. These particles may affect the abutment implant joint stability and also may alter the health of the peri-implant tissues. It was concluded that a reliable method of cleaning or using new screws should be considered prior to any clinical steps for the restoration with implant supported prostheses.

Ideas for Future Research

The following ideas may be investigated in future studies,

1. Develop a cleaning protocol for implant abutment and abutment screw

2. Measure the effect of contaminant particles on abutment screw de-torque value
3. Evaluate biological effect of using contaminated abutment screws on peri-implant tissue health.

REFERENCES

1. Binon, Paul; Sutter, Franz; Beaty, Keith; Brunski, John; Gulbransen, Harold; Weiner, Robert. The Role of Screws in Implant Systems, International Journal of Oral & Maxillofacial Implants. 1994 Special Supplement, Vol. 9, p48-63.

2. Sakaguchi, Ronald L.; Borgersen, Svenn E. Nonlinear Contact Analysis of Preload in Dental Implant Screws International Journal of Oral & Maxillofacial Implants. May/Jun1995, Vol. 10 Issue 3, p152-165.

3. McGlumphy EA, Mendel DA, Holloway JA. Implant screw mechanics. Dent Clin N Am. 1998;42:71–89.

4. Haack JE, Sakaguchi RL, Coeffy JP. Elongation and preload stress in dental implant abutment screws. Int J Oral Maxillofacial Implants. 1995;10:529–536.

5. Jörneus L, Jemt T, Carlsson L. Loads and designs of screw joints for single crowns supported by osseointegrated implants. Int J Oral Maxillofac Implants 1992;7:353–359.

6. Haack JE, Sakaguchi RL, Sun T, Coffey JP. Elongation and preload stress in dental implant abutment screws. Int J Oral Maxillofac Implants 1995;10:529–536.

7. Carr AB, Brunski JB, Hurley E. Effects of fabrication, finishing, and polishing procedures on preload in prostheses using conventional “gold” and plastic cylinders. Int J Oral Maxillofac Implants 1996;11:589–598.

8. Butignon LE1, Basilio Mde A, Pereira Rde P, Arioli Filho JN. Influence of Three Types of Abutments on Preload Values Before and After Cyclic Loading with Structural Analysis by Scanning Electron Microscopy, Int J Oral Maxillofac Implants. 2013 May-Jun;28(3):e161-70.

9. Canullo L, Micarelli C, Lembo-Fazio L, Iannello G, Clementini M. Microscopical and microbiologic characterization of customized titanium abutments after different cleaning procedures. Clin Oral Implants Res. 2014 Mar;25(3):328-36.

10. Piattelli, A., Pontes, A.E., Degidi, M. & Iezzi, G. Histologic studies on osseointegration: soft tissues response to implant surfaces and components. A review. Dent Mater. 2011 Jan;27(1):53-60.

11. Micarelli C, Canullo L, Baldissara P, Clementini M. Implant abutment screw reverse torque values before and after plasma cleaning. Int J Prosthodont. 2013 Jul-Aug;26(4):331-3.

12. Taher NM, Al Jabab AS. Galvanic corrosion behavior of implant suprastructure dental alloys. Dent Mater. 2003 Jan;19(1):54-9.

13. Cortada M, Giner L, Costa S, Gil FJ, Rodríguez D, Planell JA.Galvanic corrosion behavior of titanium implants coupled to dental alloys. J Mater Sci Mater Med. 2000 May;11(5):287-93.

14. Oh KT, Kim KN. Electrochemical properties of suprastructures galvanically coupled to a titanium implant. J Biomed Mater Res B Appl Biomater. 2004 Aug 15;70(2):318-31

15. Geurtsen W. Biocompatibility of dental casting alloys. Crit Rev Oral Biol Med. 2002;13(1):71-84. Review